Impaired mitochondrial ketone body oxidation in insulin resistant states

Elric Zweck,[a,b,c,d,k] Sarah Piel,[c,d,k] Johannes W. Schmidt,[c,d] Daniel Scheiber,[a,b,c,d] Martin Schön,[a,b,e] Sabine Kahl,[a,b,e] Volker Burkart,[a,b] Bedair Dewidar,[a,b] Ricarda Remus,[c,d] Alexandra Chadt,[b,f] Hadi Al-Hasani,[b,f] Lucia Mastrototaro,[a,b] Hug Aubin,[d,g] Udo Boeken,[g] Artur Lichtenberg,[d,g] Jörg Distler,[h] Amin Polzin,[c,d] Malte Kelm,[c,d] Ralf Westenfeld,[c,d] Robert Wagner,[a,b,e] Patrick Schrauwen,[a,b] Julia Szendroedi,[a,b,i,j] Michael Roden,[a,b,e,l] and Cesare Granata[a,b,*,l]

[a]Institute for Clinical Diabetology, German Diabetes Center, Leibniz Center for Diabetes Research, Heinrich-Heine-University Düsseldorf, Düsseldorf, Germany
[b]German Center for Diabetes Research (DZD e.V.), Partner Düsseldorf, Munich, Neuherberg, Germany
[c]Department of Cardiology, Pulmonology, and Vascular Medicine, Medical Faculty, Heinrich-Heine-University Düsseldorf, Düsseldorf, Germany
[d]CARID, Cardiovascular Research Institute Düsseldorf, Medical Faculty, Heinrich-Heine-University Düsseldorf, Düsseldorf, Germany
[e]Department of Endocrinology and Diabetology, Medical Faculty, Heinrich-Heine-University Düsseldorf, Düsseldorf, Germany
[f]Institute for Clinical Biochemistry and Pathobiochemistry, German Diabetes Center, Leibniz Center for Diabetes Research at Heinrich-Heine-University Düsseldorf, Düsseldorf, Germany
[g]Department of Cardiac Surgery, Medical Faculty, Heinrich-Heine-University Düsseldorf, Düsseldorf, Germany
[h]Department of Rheumatology and Hiller Research Institute, Medical Faculty, Heinrich-Heine-University Düsseldorf, Düsseldorf, Germany
[i]Department of Internal Medicine I and Clinical Chemistry, University Hospital Heidelberg, Heidelberg, Germany
[j]Institute for Diabetes and Cancer (IDC) and Joint Heidelberg-IDC Translational Diabetes Program, Helmholtz Center Munich, Neuherberg, Germany

eBioMedicine
2025;122: 106007
Published Online xxx
https://doi.org/10.1016/j.ebiom.2025.106007

Summary

Background Reduced mitochondrial respiratory function has been implicated in metabolic disorders like type 2 diabetes (T2D), obesity, and metabolic dysfunction-associated steatotic liver disease (MASLD), which are tightly linked to insulin resistance and impaired metabolic flexibility. However, the contribution of the ketone bodies (KBs) β-hydroxybutyrate (HBA) and acetoacetate (ACA) as substrates for mitochondrial oxidative phosphorylation (OXPHOS) in these insulin resistant states remains unclear.

Methods Targeted high-resolution respirometry protocols were applied to detect the differential contribution of HBA and ACA to OXPHOS capacity in heart, skeletal muscle, kidney, and liver of distinct human or murine cohorts with T2D, obesity, and MASLD.

Findings In humans with T2D, KB-driven mitochondrial OXPHOS capacity was ~30% lower in the heart ($p < 0.05$) and skeletal muscle ($p < 0.05$) compared to non-diabetic controls. The relative contribution of KBs to maximal OXPHOS capacity in T2D was also lower in both the heart (~25%, $p < 0.05$) and skeletal muscle (~50%, $p < 0.05$). Similarly, in kidney cortex from high-fat diet-induced obese mice, both the absolute and relative contribution of KBs to OXPHOS capacity was ~15% lower ($p < 0.05$). Finally, hepatic HBA-driven mitochondrial OXPHOS capacity was 29% lower ($p < 0.05$) in obese humans with hepatic steatosis compared to humans without.

Interpretation Mitochondrial KB-driven OXPHOS capacity is impaired in insulin resistant states in various organs in absolute and relative terms, likely reflecting impaired mitochondrial metabolic flexibility. Our data suggest that KB respirometry can provide a sensitive readout of impaired mitochondrial function in diabetes, obesity, and MASLD.

Funding German Research Foundation, German Diabetes Center, German Federal Ministry of Health, Ministry of Culture and Science of the state of North Rhine-Westphalia, German Federal Ministry of Education and Research, German Center for Diabetes Research, German Heart Foundation, German Diabetes Society, Christiane-and-Claudia Hempel Foundation, European Community and Schmutzler Stiftung.

*Corresponding author. Institute for Clinical Diabetology, German Diabetes Center, Auf'm Hennekamp 65, 40225, Düsseldorf, Germany.
E-mail address: Cesare.Granata@ddz.de (C. Granata).
[k]These authors contributed equally.
[l]These authors contributed equally.

Copyright © 2025 The Authors. Published by Elsevier B.V. This is an open access article under the CC BY-NC-ND license (http://creativecommons.org/licenses/by-nc-nd/4.0/).

Keywords: Mitochondrial respiration; Ketone bodies; Diabetes mellitus; Obesity; MASLD

Research in context

Evidence before this study

Insulin resistance is a main driver of metabolic disorders such as type 2 diabetes (T2D), obesity, and metabolic dysfunction-associated steatotic liver disease (MASLD). Accumulating evidence indicates that mitochondrial respiratory function in insulin resistant states is impaired. However, the contribution of ketone bodies (KBs) to mitochondrial oxidative phosphorylation (OXPHOS) capacity in these disease states has not been investigated, despite prior studies showing lower KB uptake in different organs in insulin resistant states. Investigating the contribution of KBs to mitochondrial capacity is relevant since KBs have been suggested to have therapeutic potential for several cardiometabolic diseases, due to their role as reserve substrates in different organs under metabolically compromised conditions.

Added value of this study

This translational study elucidated the alterations in KB-driven mitochondrial OXPHOS capacity in the above-mentioned metabolic disorders using high-resolution respirometry, the gold-standard technique for assessing OXPHOS capacity. Using different human cohorts, we identified that T2D is associated with a lower ability of cardiac and skeletal muscle mitochondria to oxidise KBs for ATP production. By utilising a murine model of diet-induced obesity, we also demonstrate decreased KB-driven OXPHOS capacity in kidney cortex. Finally, we demonstrate that the liver's ability to oxidise HBA *ex vivo* (likely in a non-physiological direction for this inherently ketogenic organ) is reduced in MASLD. The relative contribution of KBs to maximal OXPHOS capacity was also lower in all the diseased states investigated.

Implications of all the available evidence

These findings demonstrate a lower KB utilisation for mitochondrial ATP generation in T2D, obesity, and MASLD. Lower KB utilisation may represent an early sign of metabolic inflexibility for the utilisation of reserve substrates in insulin resistant states. This may therefore indicate that the therapeutic potential of increasing circulating KBs in insulin resistant states may be hampered by the reduced ability of mitochondria to utilise KBs as reserve substrates for ATP production.

Introduction

Type 2 diabetes (T2D), obesity, and metabolic dysfunction-associated steatotic liver disease (MASLD) have become increasingly common globally and are tightly associated with insulin resistance.[1] These insulin resistant states have been linked with a series of mitochondrial alterations that are thought to underpin the aetiology of these diseases.[2–5] In this regard, mitochondrial alterations in mitochondrial respiratory function and bioenergetics have been reported in the diabetic heart[6] and skeletal muscle,[7–10] the obese kidney,[11,12] and the steatotic liver.[13,14]

The ketone bodies (KBs) β-hydroxybutyrate (HBA) and acetoacetate (ACA), represent an alternative energy source for all domains of life and have attracted growing research interest[15,16] due to accumulating evidence from human and rodent studies for their therapeutic potential in various diseases, such as cardiovascular diseases,[17,18] heart failure (HF),[19,20] cardiogenic shock,[21,22] neurodegenerative disease,[23,24] kidney disease,[25,26] skeletal muscle atrophy,[27] cancer,[28] and hepatic steatosis.[15,16] However, previous studies investigating KB metabolism have not quantified the actual contribution of KBs to mitochondrial OXPHOS capacity, the main source of cellular ATP, in insulin resistant states.[29–31] Instead, most studies assessed surrogate parameters such as circulating KB concentrations,[32–34] the protein abundance or activity of enzymes involved in KB metabolism,[35–37] or tissue KB uptake.[38,39] Therefore, even though the current literature demonstrates alterations in these markers of KB metabolism in various tissues in insulin resistant states,[34–36,39–42] it remains uncertain whether this actually translates to a respectively altered contribution of KBs to mitochondrial ATP generation by OXPHOS.

We therefore hypothesised that ATP production through KB oxidation is altered in insulin resistant states. High-resolution respirometry (HRR) is the gold-standard technique for the assessment of mitochondrial OXPHOS capacity in organs and cells,[43,44] but has so far not been used to study KB metabolism in insulin resistant states. Therefore, to test our hypotheses, we validated and modified previously proposed Substrate-Uncoupler-Inhibitor Titration (SUIT) protocols[45] for HRR and utilised them to compare the contribution of KB metabolism to OXPHOS capacity of specific organs in insulin resistant conditions.[2] Our findings demonstrate a reduction in mitochondrial KB-driven OXPHOS capacity in insulin resistant states in various organs and feed into future research aiming to generate novel drugs targeting KB metabolism as a therapeutic approach.

Methods

Overview

In the present study, we first validated the feasibility of using slightly modified versions of previously proposed HRR KB protocols[45] to assess the contribution of KBs to mitochondrial OXPHOS capacity in our target organs. We initially validated these protocols in various mouse organs and later in humans; these titration protocols allowed us to also determine the specific substrate concentrations to use in each organ and species. We then applied them to different organs in distinct insulin resistant states, such as the human type 2 diabetic heart and skeletal muscle, the kidney cortex of diet-induced obese mice, and the human liver with MASLD.

Human participants and tissue acquisition

The study was performed in accordance with the Declaration of Helsinki and the STROBE guidelines and informed consent was acquired upon inclusion to the study from all participants.

Human heart studies

For initial KB protocol validation and generation of Michaelis Menten constant (K_m) plots in the human heart, ventricular tissue was acquired during cardiac surgery from end-stage HF participants undergoing left ventricular assist device (LVAD) surgery (n = 7).

For comparisons of KB-driven OXPHOS capacity between participants with T2D versus non-diabetic (Controls), the cohort included heart-transplanted individuals aged 45–70 years without clinical signs of heart failure, who underwent transcatheter ventricular endomyocardial biopsies between March 2023 and October 2024 as part of routine surveillance after heart transplantation.[46,47] Participants were divided into T2D (n = 22) and Controls (n = 35) using the following criteria for T2D: haemoglobin A1c (HbA1c) $\geq$ 6.5% or presence of specific antihyperglycemic treatment (metformin, sulfonylureas, thiazolidinedione, dipeptidyl peptidase 4 inhibitors). Cardiac tissue handling was carried out according to a previously published protocol.[47] All cardiac tissues (1–2 mg) were stored in ice-cooled biopsy preservation medium (BIOPS; composition described below) immediately after extraction until further processing. Study-related procedures have been approved by the local ethics committee at Heinrich Heine University under the study numbers 5263R, 2021-1635, and 2022-1962 (ClinicalTrials.gov Identifier: NCT05958706).

Human skeletal muscle studies

Human skeletal muscle samples were acquired from participants in the German Diabetes Study (GDS),[48] between October 2022 and April 2024. Briefly, GDS is a prospective observational clinical study that enrols individuals aged 18–69 years diagnosed with T2D within the last 12 months based on the criteria of the American Diabetes Association.[49] Samples of m. vastus lateralis were collected from T2D individuals (n = 13), and glucose-tolerant volunteers with no first-degree relatives with diabetes, who underwent a 75-g oral glucose tolerance test (AccuCheck Dextro O. G-T., Roche, Basel, Switzerland) to confirm normal glucose tolerance (n = 7, Controls). Skeletal muscle from the glucose-tolerant volunteers was also used to perform the initial KB protocol validation and generation of K_m plots. Insulin sensitivity was assessed during a mixed meal tolerance test (MMTT) using standardised liquid meals (Boost® Nestlé Health Care Nutrition, Lausanne, Switzerland) from the oral glucose insulin sensitivity (OGIS) index, as previously described and validated.[50] Approximately 50–100 mg of skeletal muscle tissue was obtained from the vastus lateralis muscle under local anaesthesia with 2% lidocaine and immediately transferred into ice-cooled BIOPS for HRR. The GDS was approved by the local ethics committee of the Medical Faculty of the Heinrich Heine University of Düsseldorf (reference number 4508) and is registered at Clinicaltrials.gov (NCT01055093).

Human liver studies

Human liver was obtained from the BARIA_DDZ cohort study (ClinTrials.gov identifier: NCT01477957), between March 2023 and December 2023. Liver biopsies were obtained by an experienced surgeon approximately 30 min after induction of anaesthesia prior to bariatric surgery according to a standardised procedure.[13] Approximately 25 mg of fresh liver tissue were immediately transferred into ice-cooled BIOPS for HRR; the remaining tissue was immediately snap-frozen in liquid nitrogen and stored at –80 °C for further analyses. Participants were divided into two groups: with (n = 11) and without (n = 5) histologically confirmed steatosis (cut-off: $\geq$5% liver lipid content). A sub-cohort was used to perform the initial KB protocol validation and generation of K_m plots in the human liver (n = 7) The BARIA_DDZ cohort study protocol was approved by the institutional ethics boards of Heinrich-Heine-University Düsseldorf (Germany) and of the North Rhine Medical Association (Germany) (no. 2022-2021_1/no. 2017222).

Laboratory mice and tissue harvest

All mouse procedures were approved by the Animal Experimental Committee of the local government "Landesamt für Natur, Umwelt und Verbraucherschutz Nordrhein-Westfalen" (LANUV) and performed in accordance with the ARRIVE guidelines for animal care and the European Convention for the Protection of Vertebrate Animals used for Experimental and other Scientific Purposes (Council of Europe Treaty Series No. 123) and 2010/63/EU. In accordance with the 3R principles (Replacement, Reduction, and Refinement), the same animals were utilised for multiple experimental steps in the development and validation of the

KB SUIT protocol to ensure the minimum number of animals necessary was used. Overall, a total of 50 mice were used in this study.

Protocol validation in mice

These experimental procedures were carried out in accordance with Directive 2010/63/EU on the protection of animals used for scientific purposes (§ 4 Absatz 3 des Tierschutzgesetzes) and were approved by the internal animal officer (Tierschutzbeauftragter) of the DDZ. Mice used for protocol validation, generation of K_m plots, and characterisation of our combined KB SUIT protocol were female wildtype C57BL/6J mice aged 16–26 weeks (n = 12). Mice were fed with a standard chow diet and provided tap water ad libitum. For tissue harvest, mice were sacrificed, and organs were immediately collected and processed for HRR (see below).

Kidney cortex of diet-induced obese mouse studies

For these experiments (LANUV AZ: 81-02.04.2021/A218), male wildtype C57BL/6J mice aged 10–12 weeks were obtained from Janvier-Labs and housed at the Zentrale Einrichtung für Tierforschung und wissenschaftliche Tierschutzarbeit (ZETT) animal facility of the Heinrich-Heine-University Düsseldorf. This mouse strain shows a high susceptibility to develop obesity and insulin resistance in response to high-fat diet (HFD).[51,52] Male mice were chosen because they are less protected from obesity-induced renal dysfunction.[53] Baseline body weight was not directly measured prior to the start of the dietary intervention. However, all mice were male, of the same strain, and were purchased from the same Vendor at the same age. Mice were randomly assigned to cages, and cages were then randomly allocated to provide either a HFD (Sniff, S7200-E010, 60 kJ % fat) to induce diet-induced obesity (DIO, n = 12) or a normal chow diet (Sniff, V1184-300, 16 kJ% fat) as controls (n = 10), for 24 weeks each. Both treatment groups received food and tap water ad libitum. The health of the animals was monitored using a scoring sheet that assessed body weight, overall condition, and behaviour. Animals exhibiting severe distress before completion of the treatment period were euthanised. After 24 weeks of HFD or normal chow diet, mice were sedated with an I.P. injection of ketamine (100 mg/kg; Pfizer Pharma) and xylazine (10 mg/kg; Bayer AG). Blood was collected by cardiac puncture and the left kidney was immediately harvested and prepared for HRR, as described below. Plasma insulin levels were determined with the Ultra Sensitive Mouse Insulin ELISA Kit (90,080; Crystal Chem Europe, Zaandam, Netherlands), according to the manufacturer's instructions. All personnel involved in the experiments and downstream analyses were blinded to group assignments.

Sample size in diseased-state cohorts

For these exploratory studies, which employed respirometry protocols specifically developed to investigate the contribution of KBs to OXPHOS capacity, no formal power calculation was performed prior to initiation due to the lack of available effect size data. Instead, despite its limitations, we applied the resource equation method,[54] which yielded estimated required numbers of participants/animals (E) of 55 for the human heart, 18 for the human skeletal muscle, 20 for the murine kidney, and 13–14 for the human liver. According to this method, these values represent adequate sample sizes (E > 10) to detect significant differences. All human tissues were gathered from participants of ongoing, prospective cohort studies in the pre-specified time frames stated in each respective section, according to set collaboration agreements. Samples for the DIO mouse study cohort were also gathered from mice of an ongoing collaboration study. The results presented are based on the initial analyses of the respective datasets, with no additional participants or mice included thereafter.

Cell culture

Primary hepatocyte experiments

Mouse primary hepatocytes. Mouse primary hepatocytes were isolated from 16- to 20-week-old mixed-sex C57BL/6J mice (HBA titration: n = 6, ACA titration: n = 7) as previously described,[55] with minor modifications. After cervical dislocation, the liver was rapidly exposed and perfused sequentially with EGTA and collagenase solutions through the vena cava at 37 °C. The digested liver was minced gently in suspension buffer and filtered through a 100 μM cell strainer (Corning, Wiesbaden, Germany). Single-cell hepatocytes were separated by low-speed centrifugation at 50*g* for 2 min, further purified by Percoll® density gradient (Sigma–Aldrich, Taufkirchen, Germany), and finally suspended in William medium supplemented with 1% penicillin/streptomycin and 10% FBS. Cell viability was assessed by trypan blue dye exclusion. With this protocol, we have previously shown mouse hepatocytes purity to be >98.5%.[56] After cell counting, primary hepatocytes were suspended directly in mitochondrial respiration medium (MiRO5; for chemical composition see below) and immediately added to the Oxygraph-2k chambers (Oroboros Instruments, Innsbruck, Austria) at a concentration of 100,000 cells/mL.

Human primary hepatocytes. Human primary hepatocytes from n = 3 females were obtained from commercial sources (LifeNet Health®, Virginia Beach, VA, USA). These commercially available hepatocytes are isolated from human liver with an improved protocol of the gold-standard method for hepatocyte isolation.[57] After thawing and washing, cell viability was assessed by trypan blue dye exclusion, and after cell counting, primary hepatocytes were suspended directly in MiRO5 and immediately added to the Oxygraph-2k chambers (Oroboros Instruments, Innsbruck, Austria) at a concentration of 250,000 cells/mL.

High-resolution respirometry

Sample preparation

Heart, skeletal muscle, and liver tissues were collected in ice-cooled BIOPS (containing [in mM]: 2.77 CaK_2EGTA, 7.23 K_2EGTA, 20 imidazole, 20 taurine, 50 4-morpholine-ethanesulfonic acid, 0.5 dithiothreitol, 6.56 $MgCl_2$·6H2O, 5.77 Na_2ATP, and 15 disodium phosphocreatine, pH 7.1), whereas kidney cortex was collected in ice-cooled MiR05 (containing [in mM unless specified]: 0.5 EGTA, 3 MgCl2, 60 K-lactobionate, 20 taurine, 10 KH_2PO_4, 20 HEPES, 110 sucrose and 1 g/L BSA essentially fatty acid-free, pH 7.1) for immediate preparation for HRR.[58–62]

Sample preparation for HRR was carried out according to standard protocols. In short, fresh cardiac[58] and skeletal muscle fibres[61] were mechanically separated in ice-cold BIOPS using forceps; fresh kidney cortex[62] was cut into small pieces and gently tapped with forceps in ice-cold MiRO5; fresh liver was cut in ~2 × 2 mm pieces using forceps in ice-cold BIOPS,[59,60] under a light microscope. Subsequently, samples were chemically permeabilised by gentle agitation for 20 min at 4 °C with saponin dissolved in BIOPS (myocardium and skeletal muscle) or MiRO5 (kidney cortex) at a concentration of 50 µg/mL, except for kidney cortex for which 100 µg/mL of saponin was used.[62] For both human and mouse myocardium samples, the saponin step lasted 30 min.[58] As previously indicated for the liver, chemical permeabilization was not performed.[59,60] For all tissues, this was followed by three 5-min (or two 10-min for myocardium samples) washing steps in ice cold MiRO5. Cells (primary hepatocytes) were added directly to the chambers and—following an initial stabilisation—were permeabilised with 50 µg/million cells of digitonin in the presence of malate and ADP.[63]

High-resolution respirometry

Mitochondrial respiration was measured in duplicates (except for K_m determinations) in MiR05 at 37 °C, 750 rpm stirrer speed and a chamber volume of 2.0 mL using the high-resolution Oxygraph-2k (Oroboros Instruments, Innsbruck, Austria). For all tissues, oxygen concentration was maintained, via direct syringe injection of pure O_2, between 270 and 480 nmol mL^{-1} for the duration of the experiment, to avoid potential oxygen diffusion limitations.[64] Mitochondrial respiration in cells was instead assessed at sub-atmospheric oxygen pressure (50 and ~195 nmol mL^{-1}). Cytochrome *c* (10 µM) was added to assess the integrity of the outer mitochondrial membrane.[65] Inclusion criteria for all cohorts included valid respirometry measurements according to the following prespecified criteria: i) a cytochrome *c* <15% in at least one chamber[66] and ii) a positive response to OXPHOS substrates of the fatty acid oxidation (F), NADH (N), and/or succinate (S) pathway. Only samples with available mitochondrial respiration traces were included in our analyses.

Validation of HBA and ACA as HRR substrates in target organs

Since HBA and ACA have previously been used as HRR substrates in murine skeletal and cardiac muscle, as well as in human skeletal muscle,[45] but not in the other target organs or cohorts of our study, we first validated their suitability for our research. We then used titration protocols to determine the optimal substrate concentration for each organ and species for the subsequent translational comparison studies.

HBA is oxidised to ACA by β-hydroxybutyrate dehydrogenase (BDH1) during the first step of ketolysis. During this reaction, NAD^+ is reduced to NADH, which can directly enter the electron transport system (ETS) via complex I (CI) (Fig. 1); hence, addition of malate is not required. Therefore, after adding saturating levels of ADP (5 mM) and obtaining stabilisation of respiration (times ranging from 10 to 60 min depending on tissues, likely due to exhaustion of endogenous substrates), sodium DL-β-hydroxybutyrate (Sigma–Aldrich, cat. no.: H6501-5G; racemic mixture of D and L isoforms) was titrated stepwise from 0.01 mM up to 20–60 mM to stimulate mitochondrial respiration through BDH1 ($[HBA]_P$; Fig. 1 yellow shaded area). The resulting JO_2 and corresponding K_m values of permeabilised mouse heart, skeletal muscle (soleus), and kidney cortex, and permeabilised human heart and skeletal muscle (vastus lateralis) are presented in Supplementary Figure S1a–g. The liver JO_2 and K_m values are shown in the relevant Results section.

ACA degradation is catalysed by succinyl-CoA: 3-ketoacid (oxoacid) coenzyme A transferase (SCOT), which in the second step of ketolysis converts ACA and succinyl-CoA to ACA-CoA and succinate (Fig. 1). Unlike BDH1, SCOT requires assistance from the TCA cycle (via addition of a TCA cycle substrate; e.g., malate) to provide sufficient concentrations of succinyl-CoA along with ACA. Therefore, for ACA titration protocols, we first added saturating levels of ADP (5 mM) and malate (2 mM), obtained stabilisation of respiration and subsequently titrated lithium acetoacetate (Sigma–Aldrich, cat. no.: A8509-10MG) stepwise from 0.005 mM to 15–30 mM, to stimulate mitochondrial respiration through SCOT ($[ACA + M]_P$; Fig. 1, blue shaded area). The resulting JO_2 and K_m values of permeabilised mouse heart, skeletal muscle (soleus), and kidney cortex and permeabilised human heart and skeletal muscle (vastus lateralis) are presented in Supplementary Figure S1h–n. The liver JO_2 and K_m values are shown in the relevant Results section. Of note, ACA (and HBA) was made fresh each day and was used within 4 h to avoid decarboxylation and subsequent degradation.[67]

To rule out effects of osmolarity changes resulting from the addition of HBA and ACA, provided as sodium (NaHBA) and lithium (LiACA) salts, respectively, on JO_2 values, we performed a series of titrations in all

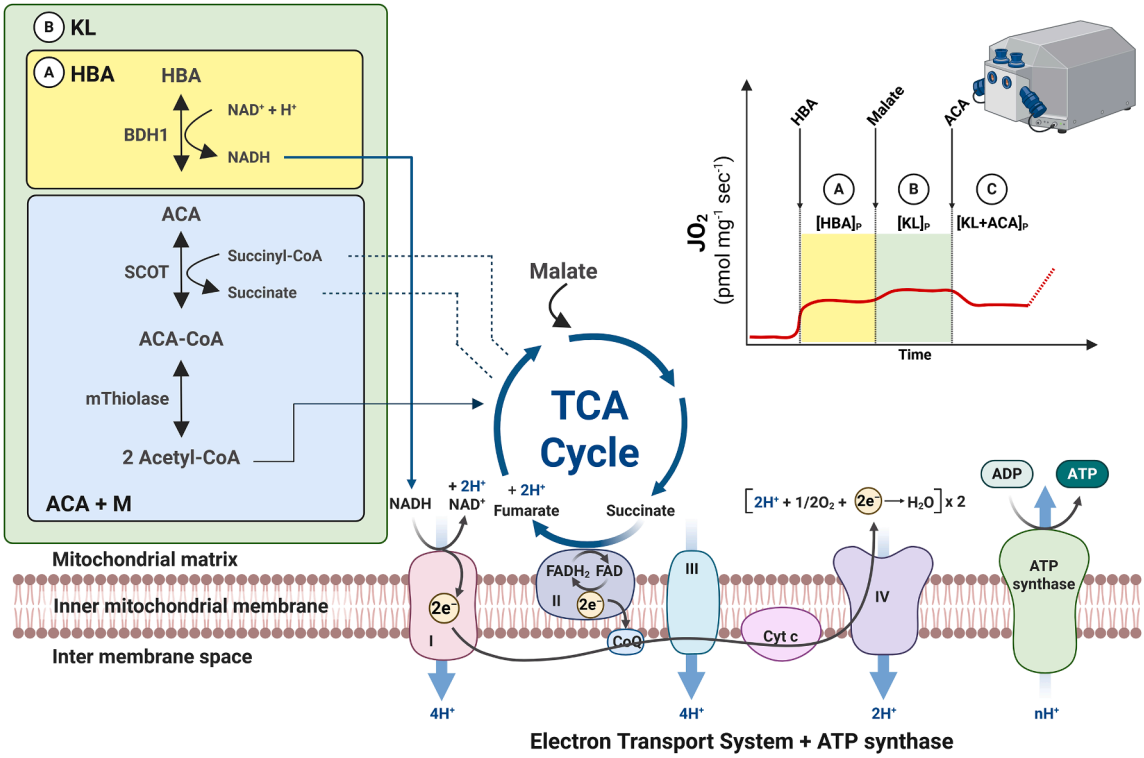

***Fig. 1:* Pathways of ketone body-linked ATP generation by mitochondrial oxidative phosphorylation.** Ketone body oxidation is initiated by addition of β-hydroxybutyrate (HBA) in the presence of ADP (yellow shaded area); complete ketolysis is achieved by further addition of malate (M; green shaded area); further addition of acetoacetate (ACA) allows further insight into the interplay of the various enzymes involved in ketolysis (for a detailed explanation, see Methods). The isolated contribution of ACA to ketolysis can be achieved by addition of ACA and M in the presence of ADP (blue shaded area). ADP: adenosine diphosphate; ATP: adenosine triphosphate; BDH1: β-hydroxybutyrate dehydrogenase; CoA, coenzyme A; CoQ: coenzyme Q; e^-: electron; $FADH_2$: flavin adenine dinucleotide; H^+: proton; JO_2: oxygen flux; KL: ketolysis; NADH: nicotinamide adenine dinucleotide; P: phosphorylating (coupled) mitochondrial respiration state; SCOT: Succinyl-CoA: 3-ketoacid (oxoacid) coenzyme A transferase; TCA: tricarboxylic acid cycle. Figure generated using BioRender.com (Toronto, CA).

the tissue investigated (n = 3, mixed-sex, 17 weeks old C57BL/6J mice). In these experiments, NaHBA (or LiACA) was added to chamber A and NaCl (or LiCl) to chamber B, enabling simultaneous measurements in parallel chambers. Results indicate no osmolarity effects on JO_2 values at the highest concentration of NaHBA and LiACA used in our SUIT protocols (Supplementary Figure S2).

Combined ketone body SUIT protocol

To assess the association of insulin resistant states with KB oxidation in HRR, we devised a combined KB SUIT protocol incorporating both HBA and ACA that can quantify the complete contribution of ketolysis to OXPHOS and the interplay between the different ketolytic enzymes within a single analysis. To determine the initial step of ketolysis ($[HBA]_P$, where P indicates phosphorylation; Fig. 1, yellow shaded area), saturating ADP concentrations (5 mM) were added, followed by brief stabilisation and subsequent injection of a single dose of saturating HBA, pre-determined via the above-mentioned HBA-titration protocols, to stimulate maximal HBA-linked OXPHOS capacity. For ketolysis to proceed, sufficient supply of succinyl-CoA to SCOT is required; this was achieved by subsequent addition of the TCA cycle metabolite malate (2 mM), which if added by itself has negligible impact on OXPHOS.[68] Because this step encompasses complete ketolysis, we named this respiratory state "$[KL]_P$" (Fig. 1, green shaded area). To gain further insight into the relative contribution of the various enzymes involved in ketolysis, we included a third step, whereby ACA can be titrated stepwise or added in a single injection. We named this readout "$[KL + ACA]_P$". The ratio between $[KL]_P$ and $[KL + ACA]_P$ ($[KL]_P$/$[KL + ACA]_P$) allows to determine whether and to which extent the activity of specific ketolytic enzymes may be rate limiting. In this regard, a ratio below 1 suggests that addition of ACA provides further substrate for the reaction catalysed by SCOT/mThiolase, suggesting BDH1 would be rate limiting. A ratio above 1 suggests a product-induced inhibition of the equilibrium of the

reaction catalysed by BDH1 (Le Chatelier's principle), since its product (ACA) is now provided at greater concentrations; this would indicate that SCOT/mThiolase do not possess a "reserve capacity" to further drive ketolysis. Thus, a higher $[KL]_P/[KL + ACA]_P$ ratio may suggest a lower ability to utilise excess ACA over the already present HBA. When KB-supported mitochondrial respiration is low, the [KL]/[KL + ACA] ratio should be interpreted with caution, as it may not reliably reflect meaningful differences in BDH1 relative to SCOT activity.

After these KB states, 5 mM pyruvate (except human and mouse myocardium) and 10 mM glutamate ($[KL + ACA + N]_P$), and 10 mM succinate ($[KL + ACA + NS]_P$) were added to test the samples' response to non-KB substrates. Leak respiration (L) was subsequently assessed by addition of the ATP synthase inhibitor oligomycin (2.5 μM, except human heart: 5 μM; $[KL + ACA + NS]_L$) (except for human skeletal muscle). Maximal uncoupled respiratory ETS (E) capacity ($[KL + ACA + NS]_E$) was assessed by stepwise titration with the protonophore FCCP (0.75–1.5 μM). The CIII inhibitor antimycin A (5 μM) was finally added to determine non-mitochondrial oxygen consumption (ROX). A detailed description of the substrates, inhibitors, and uncoupler concentrations used for the combined KB SUIT protocol is presented in Supplementary Tables S1 and S2 for all mouse and human organs tested, respectively. The resulting JO_2 values of permeabilised mouse heart, skeletal muscle (soleus), and kidney cortex are presented in Supplementary Figure S3. Owing to the inability of hepatocytes to undergo ketolysis due to the lack of SCOT,[69] our combined KB SUIT protocol is unsuitable for hepatic tissue, as the respiratory states $[KL]_P$ and $[KL + ACA]_P$ cannot be achieved; hence, we did not use it in the liver.

NADH and succinate-linked (NS) and fatty acid, NADH, and succinate-linked (FNS) SUIT protocols

NS or FNS protocols were used as surrogates of maximal coupled OXPHOS capacity to calculate the ratios of KB-linked respiration relative to maximal OXPHOS capacity. 5 mM pyruvate, 10 mM glutamate, and 10 mM succinate (as well as 1.0 mM octanoylcarnitine in the heart) were added in the presence of saturating ADP (5 mM) to stimulate P with limitation of flux by convergent electron input via the N and S pathway. Substrates of the F pathway were only added in the heart protocols due to its higher physiological reliance on fatty acids,[6,70] to stimulate P with limitation of flux by convergent electron input via the F, N and S pathway. Of note, when substrates of the F, N, and S pathways were added after KB substrates, the resulting JO_2 values were mostly significantly lower than in similar protocols without prior addition of KB (Supplementary Figure S4). Thus, maximal OXPHOS capacity determined from KB + FNS and FNS protocols should not be used interchangeably to ensure the internal validity of the calculated ratios. However, using a KB + FNS protocol to determine maximal OXPHOS capacity remains a valuable approach when tissue or machine availability is limited. In the present study, this was the case for the kidney cohort, where, due to a shortage of machine availability, the combined KB SUIT protocol described above was used.

Tissue homogenisation

Briefly, proteins were extracted from ~20 mg of frozen tissues and homogenised in 200 μl of lysis buffer (25 mM trisaminomethane-hydrochloride (Tris–HCl), 1 mM ethylenediaminetetraacetic acid (EDTA), 150 mM NaCl, 0.2% Tergitol) with protease (cOmplete Tablets, EASYpack, Roche Diagnostics) and phosphatase (PhosSTOP, EASYpack, Roche Diagnostics) inhibitors. Samples were shaken thrice for 1 min at 20 Hz in a TissueLyser II (Qiagen) and centrifuged (13,000 rpm, 15 min, 4 °C) to pellet insolubilised material. The concentration of the extracted proteins was determined in the supernatant using the bicinchoninic acid (BCA) Assay Kit (Thermo Scientific, Dreieich, Germany). Tissue homogenates were subsequently used for both citrate synthase (CS) activity measurements and immunoblotting.

Citrate synthase activity

CS activity was assayed spectrophotometrically by a commercially available kit (Citrate Synthase Assay Kit; Sigma–Aldrich, St. Louis, MO, USA), according to Morgunov and Srere[71] and is expressed as [nmol min^{-1} mg $tissue^{-1}$].

Immunoblotting

Expression levels of proteins of interest were assessed by immunoblotting, as previously described.[72] Aliquots of 20 μg of total proteins were diluted 4 times with reducing Laemmli sample buffer containing 2-mercaptoethanol (1610747, Biorad, CA, USA), boiled 5 min at 95 °C and then loaded onto a SDS-polyacrylamide gradient gel (4–20% Mini-PROTEAN® TGX™ Stain-Free Gels, Biorad, CA, USA). Prior to immunoblotting the stain-free gels were UV-activated for 1 min and pictures were taken using the ChemiDoc MP imaging system (Biorad, CA, USA). Proteins were transferred to a polyvinylidene difluoride membrane using the Trans-Blot Turbo Transfer System (Biorad, CA, USA), imaged using the ChemiDoc MP and quantified using Image Lab™ 6.0.1 software (Bio-Rad, CA, USA) for normalisation. The membranes were blocked in 5% milk in Tris-buffered saline-Tween (TBS-T) for 2 h at room temperature and then they were incubated overnight at 4 °C with the primary antibodies diluted 1:1000. On the next day, membranes were washed with TBST buffer and incubated for 1 h at room

temperature with a horseradish peroxidase-conjugated secondary anti-rabbit antibody, diluted 1:2500. The sources and catalogue numbers of the respective antibodies are provided in Supplementary Table S3. The membranes were finally coated with Immobilon Western Chemiluminescent HRP Substrate (Merck Millipore, Darmstadt, Germany) and the proteins were detected using the ChemiDoc MP in combination with ImageLab for densitometric analysis. Immunoblot data were normalised to total protein quantification obtained from stain-free membrane imaging (loading control) and expressed in arbitrary units. For analysis and comparison of samples on different gels, an inter-run calibrator (IRC) was loaded as reference sample on each gel to correct for gel-to-gel variation.[73]

Statistical analysis

Statistical analyses were performed using GraphPad Prism version 10.0.1 (GraphPad Software, San Diego, California, USA) or R version 4.3.0 (R Foundation for Statistical Computing, Vienna, Austria). All values in figures are reported as mean ± SEM. In tables showing cohort characteristics, data are presented as median with the interquartile ranges or as total number and proportion. Standard distribution was assessed using Shapiro–Wilk tests and visually using normal QQ plots and histograms. Michaelis–Menten kinetics were calculated by subtracting values of mitochondrial respiration prior to first titration of the respective substrate (HBA or ACA) from all values. For comparison of different respiratory states within a single protocol, repeated measurement mixed-effects models (REML) were used with post-hoc pairwise between-group tests. Post-hoc tests were corrected for multiple testing based on the false discovery rate, in that p values were reported as significant only in cases were the q value was below 0.05.[74] Simple comparisons between groups without repeated measurements were carried out using paired parametric (paired t-test), paired non-parametric (Wilcoxon signed-rank test), unpaired parametric (Welch's t-test), or unpaired non-parametric (Mann-Whitney-Test or Fisher's exact test) tests, as specified in the respective figure legends and table footnotes, and according to the underlying study cohort and distribution, respectively. Differences in medians between human groups were analysed using the Hodges-Lehmann Estimator with 95%-confidence intervals; differences in proportions between human groups using the Newcombe-Wilson Score with Continuity Correction for 95% confidence intervals. Univariate linear regression models were used to assess the associations of insulin sensitivity and KB respiratory states in human skeletal muscle. Multiple linear regression analyses using the least squares method were performed for respiratory outcomes adjusting for the covariates age and body mass index (BMI) in the human groups. Sex-stratified analysis of mitochondrial respiration was conducted for the human cohorts with sufficient group size after sex stratification. An alpha level of 0.05 was considered statistically significant. In figures where multiple testing was corrected using the false discovery rate, values reflecting statistically significant differences ($q < 0.05$) are indicated with an asterisk (*). All p-values are reported in figures and tables, while only p-values indicating statistically significant differences ($p < 0.05$) are reported in the Results.

Role of funders

The funders were not involved in the design of the study, data collection, analysis or interpretation, and had no role in writing the manuscript.

Results

To determine the contribution of ketolysis to OXPHOS and the interplay between the different ketolytic enzymes in T2D, obesity, and MASLD, we devised a combined KB SUIT protocol consisting of the sequential addition of i) HBA to assess $[HBA]_P$ (Fig. 1, yellow shaded area), ii) malate, to assess complete ketolysis ($[KL]_P$; Fig. 1, green shaded area), and iii) ACA, to assess potential differences in the activity of distinct ketolytic enzymes ($[KL + ACA]_P$; Fig. 1 & Methods).

Lower ketone body-dependent OXPHOS capacity in the type 2-diabetic heart

We employed our combined KB SUIT protocol in human ventricular myocardium derived from humans with and without T2D undergoing routine endomyocardial biopsies after heart transplantation. Persons with T2D presented with higher HbA_{1c}, BMI, and circulating non-esterified fatty acids than controls and a higher proportion of participants in the T2D group were treated with antihyperglycemic treatments such as metformin, dipeptidyl peptidase (DPP4) inhibitors, sodium-glucose co-transporter 2 (SGLT2) inhibitors and insulin therapy; the two groups did not differ in any other demographic characteristics (Supplementary Table S4).

Participants with T2D presented with 24% and 32% lower JO_2 values in the KB-linked respiratory states $[KL]_P$ and $[KL + ACA]_P$, respectively (both $p < 0.05$; Fig. 2a). With respect to alterations in mitochondrial respiration driven by non-KB substrates, consistent with previous observations by our and other groups,[6,75,76] we observed a numerically, but not significantly reduced OXPHOS capacity for the respiratory states $[F]_P$, $[FN]_P$, and $[FNS]_P$ in the T2D group (Fig. 2b). To gain further insight into the relative contribution of KB metabolism to maximal coupled OXPHOS capacity, we calculated the ratios between the three states of KB-linked mitochondrial respiration (Fig. 2a) and the maximal coupled OXPHOS capacity achieved during the FNS protocol ($[FNS]_P$; Fig. 2b). We observed a

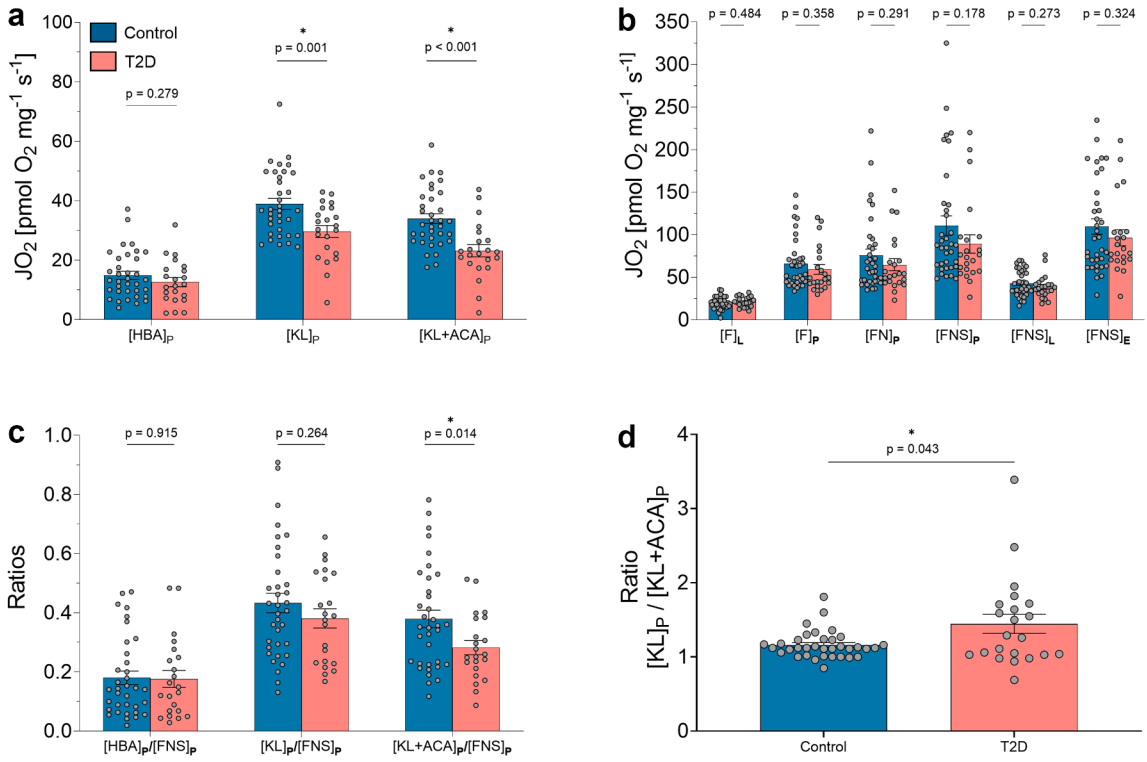

Fig. 2: **Reduced ketone body dependent OXPHOS capacity in the diabetic heart.** Mitochondrial respiration (JO_2) of permeabilised ventricular myocardium of heart transplant recipients undergoing routine endomyocardial biopsy without (Control) versus with Type 2 Diabetes (T2D), obtained with (a) the combined ketone body (KB) and (b) the fatty acid oxidation (F), NADH (N), and succinate (S) combined (FNS) pathway mitochondrial respiration protocols. (c) Relative contribution of the different respiratory states of KB-linked versus maximal coupled FNS-linked mitochondrial respiration. (d) $[KL]_P/[KL + ACA]_P$ ratio. a–c: repeated-measurements mixed-effects (REML) model with correction for multiple testing with the false discovery rate.[74] d: Welch's t-test. n = 35 (control) versus 22 (T2D). Data are mean ± SEM. HBA: β-hydroxybutyrate; $_E$: electron transport chain capacity (noncoupled) mitochondrial respiration state; JO_2: oxygen flux; KL: ketolysis; $_L$: leak mitochondrial respiration state; $_P$: phosphorylating (coupled) mitochondrial respiration state.

significant reduction in the ratio $[KL + ACA]_P/[FNS]_P$ in T2D (p = 0.014; Fig. 2c). Additionally, the ratio $[KL]_P/[KL + ACA]_P$ was greater than 1 and higher in T2D (p = 0.043; Fig. 2d). The decrease in the two respiratory states involving the enzyme SCOT ($[KL]_P$ and $[KL + ACA]_P$) along with the reduction in the $[KL + ACA]_P/[FNS]_P$ ratio in T2D, coupled with the increase in the $[KL]_P/[KL + ACA]_P$ ratio, suggests that impaired KB oxidation in the diabetic heart may be driven more by the reduced ability of SCOT to metabolize ACA than by the ability of BDH1 to metabolize HBA. Separate sensitivity analyses showed consistency with these findings in male and female participants (Supplementary Figure S5) and in participants with and without SGLT2 inhibitor therapy (Supplementary Figure S6). Due to the potential confounding effects of age and BMI, we performed linear regression analyses for all respiratory outcomes, which also presented comparable results (Supplementary Table S5). Finally, when measured across both groups, HbA_{1c} levels were inversely correlated with $[KL]_P$ (Spearman r = –0.262, p = 0.049) and $[KL + ACA]_P$ (Spearman r = –0.287, p = 0.031) (Supplementary Figure S7). Taken together, these results indicate that KB-linked mitochondrial respiration is lower in the diabetic heart, particularly with respect to ACA-driven respiration. Future research should investigate the temporal dynamics of cardiac KB-linked and FNS-linked mitochondrial ATP production changes during T2D progression.

Lower KB-dependent mitochondrial OXPHOS capacity in the type 2-diabetic skeletal muscle

Impaired mitochondrial oxidative function and mitochondrial metabolic flexibility, a mechanism by which an organ's mitochondria adapt to altered bioenergetic demands,[13] have previously been shown in skeletal muscle of T2D when compared to glucose-tolerant humans.[2,3] Here, we aimed to investigate if the capacity to utilise KBs for ATP production in skeletal muscle of humans with T2D is also lower. Study participants with and without T2D[77] did not differ with respect to demographic characteristics, such as age, sex, or BMI

(Supplementary Table S6). Similar to findings in the human diabetic heart, our combined KB SUIT protocol revealed lower KB-linked OXPHOS capacity in humans with T2D in the $[KL]_P$ and the $[KL + ACA]_P$ state (both $p < 0.05$; Fig. 3a). In parallel, we report no difference in maximal OXPHOS capacity between humans with and without T2D in the NS pathway mitochondrial respiration protocol (Fig. 3b). Although most studies have shown a decrease in maximal OXPHOS capacity in diabetes,[7,9,78,79] our results are consistent with previous work indicating no difference in NS-driven OXPHOS capacity in participants with obesity and diabetes versus participants without diabetes.[80] As a consequence of the above findings, the relative contribution of KBs to maximal coupled OXPHOS capacity was 48–58% lower in T2D compared to non-diabetic controls in all three KB-linked respiration states (all $p < 0.05$; Fig. 3c). The $[KL]_P/[KL + ACA]_P$ ratio was higher in T2D ($p = 0.038$; Fig. 3d); although these findings should be interpreted with caution given the overall low JO_2 response, they may potentially reflect an impaired SCOT-mediated degradation of additional ACA at saturating HBA concentrations in diabetic skeletal muscle. A separate sensitivity analysis in participants not receiving SGLT2 inhibitors showed results consistent with the main findings (Supplementary Figure S8). Similarly, linear regression analysis adjusting for age and BMI yielded comparable results or trends (Supplementary Table S7). Finally, insulin sensitivity, as assessed using the OGIS index,[50] was associated with $[KL]_P/[NS]_P$ ($R^2 = 0.451$, $p = 0.024$) and presented a similar trend with $[HBA]_P/[NS]_P$ ($R^2 = 0.297$, $p = 0.083$) (both Supplementary Figure S9). Overall, these findings indicate a reduced ability of skeletal muscle mitochondria to utilise KBs as a substrate to generate ATP through OXPHOS in individuals with T2D as compared to those without T2D, supporting the concept of impaired mitochondrial metabolic flexibility in skeletal muscle of humans with T2D and insulin resistance.[2,3]

To assess whether these functional differences stemmed from changes in mitochondrial content, we measured CS activity, a validated biomarker of mitochondrial abundance,[81] and found no differences between groups (Fig. 3e). Following normalisation to CS activity, respiratory values showed trends similar to the non-normalised values (Fig. 3a and b), although no significant differences were detected (Supplementary Figure S10). Moreover, there was no difference between groups in the protein content of the key ketolytic enzymes BDH1 and SCOT (Fig. 3f; Supplementary Figure S11). Taken together, these findings suggest that the observed changes in KB-linked mitochondrial OXPHOS capacity were not attributable to differences in mitochondrial content or in BDH1 and SCOT

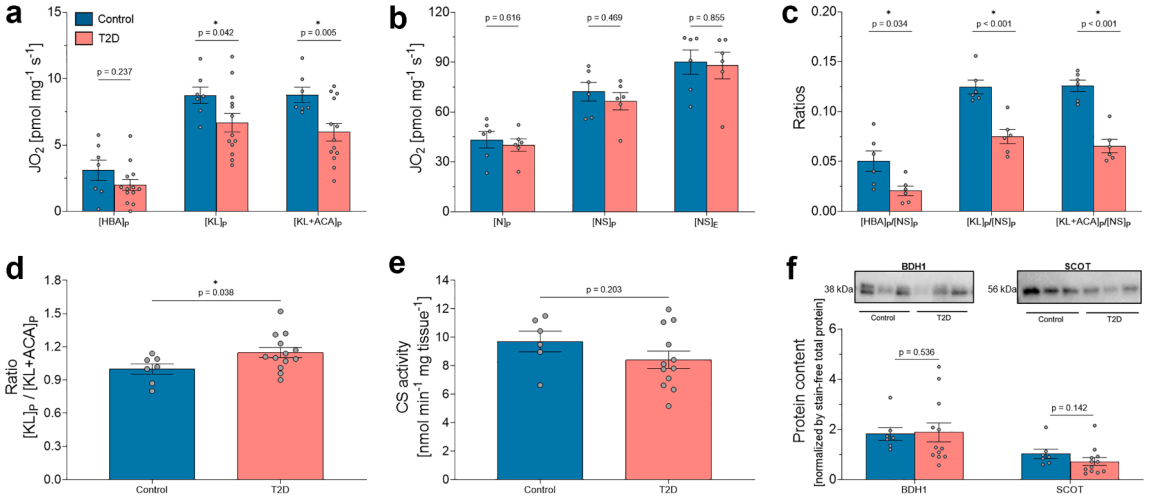

***Fig. 3:* Lower KB-dependent mitochondrial OXPHOS capacity in the type 2-diabetic skeletal muscle.** Mitochondrial respiration (JO_2) in permeabilised skeletal muscle (vastus lateralis) fibres from type 2 diabetes (T2D) versus glucose-tolerant (Control) individuals, obtained with (a) the combined ketone body and (b) the NADH (N) and succinate (S) combined (NS) pathway mitochondrial respiration protocols. (c) Relative contribution of the different respiratory states of KB-linked versus maximal coupled NS-linked mitochondrial respiration. (d) $[KL]_P/[KL + ACA]_P$ ratio. Analysis of (e) Citrate Synthase (CS) activity, a marker of mitochondrial content, and (f) protein expression of β-hydroxybutyrate dehydrogenase (BDH1) and succinyl-CoA: 3-ketoacid (oxoacid) coenzyme A transferase (SCOT). Representative immunoblots of BDH1 and SCOT from three replicates of each group are shown. a, d: n = 7 versus 13. b, c: n = 6 versus 6, e: n = 6 versus 12, f: n = 7–12. a–c: repeated-measurements mixed-effects (REML) model with correction for multiple testing with the false discovery rate.[74] d and e: Welch's t-test. f: Mann-Whitney-Test. Data are mean ± SEM. HBA: β-hydroxybutyrate; $_E$: electron transport chain capacity (noncoupled) mitochondrial respiration state; JO_2: oxygen flux; KL: ketolysis; $_L$: leak mitochondrial respiration state; $_P$: phosphorylating (coupled) mitochondrial respiration state.

protein expression, but were more likely related to functional deficits in mitochondrial KB metabolism.

Lower KB-dependent OXPHOS capacity in the kidney cortex of diet-induced obese male mice

Increasing evidence suggests that mitochondrial alterations associated with insulin resistant states are not only found in cardiac and skeletal muscle, but also in the kidney.[11,82] Furthermore, altered renal mitochondrial function is a pathological mediator of kidney disease,[83] and T2D is associated with altered kidney function.[11,84] Finally, KBs may possess reno-protective properties due to their ability to reduce renal oxidative stress and apoptosis, and to promote anti-inflammatory proteins.[82] Given the above background, we sought to investigate if renal KB-driven mitochondrial respiration is also affected by obesity and insulin resistance. In the absence of fresh human kidney cortex, we utilised our combined KB respirometry protocol to investigate potential alterations in KB-linked mitochondrial respiration in the kidney cortex of a DIO C57BL/6J mouse model reflecting obesity and prediabetes,[85] both of which are tightly associated with insulin resistance. Mouse characteristics are presented in Supplementary Table S8. In DIO mice, plasma insulin levels, a marker of insulin resistance, were more than 5 times higher compared to controls ($p = 0.002$).

Absolute KB-linked respiration was lower in DIO mice compared to controls for all KB respiratory states (all $p < 0.05$; Fig. 4a), suggesting that these metabolic conditions reduce the ability of renal cortex to generate ATP from KBs. No difference between groups was reported following the subsequent addition of NS pathway substrates ($[KL + ACA + NS]_P$: 237.56 ± 45.26 and 240.46 ± 71.86 pmol s^{-1} mg^{-1} for control and DIO mice, respectively; $p = 0.910$, unpaired Welch's t test). As a consequence, the relative contribution of KB-driven respiratory states to maximal coupled OXPHOS capacity was also reduced in DIO versus controls for all KB respiratory states (all $p < 0.05$; Fig. 4b). The $[KL]_P/[KL + ACA]_P$ did not differ between groups (Fig. 4c). Taken together, these findings demonstrate that obesity-induced insulin resistance results in a reduced ability of renal mitochondria to utilise KBs for ATP production by OXPHOS.

To determine if variations in mitochondrial content could explain these functional differences, we quantified CS activity, and observed no group differences (Fig. 4d). When respiratory values were normalised to CS activity, the patterns mirrored those of the unadjusted data (Fig. 4a), but failed to reach statistical significance (Supplementary Figure S12). In contrast, the protein expression of BDH1 and SCOT was reduced in the kidney cortex of DIO mice (both $p < 0.05$, Fig. 4e and f; Supplementary Figure S13), further corroborating mitochondrial functional reductions. Taken together, these findings suggest that the mitochondrial functional impairments related to KB metabolism in the DIO kidney may be due to defects in key enzymes of the ketolytic machinery, rather than to an overall reduction in mitochondrial content.

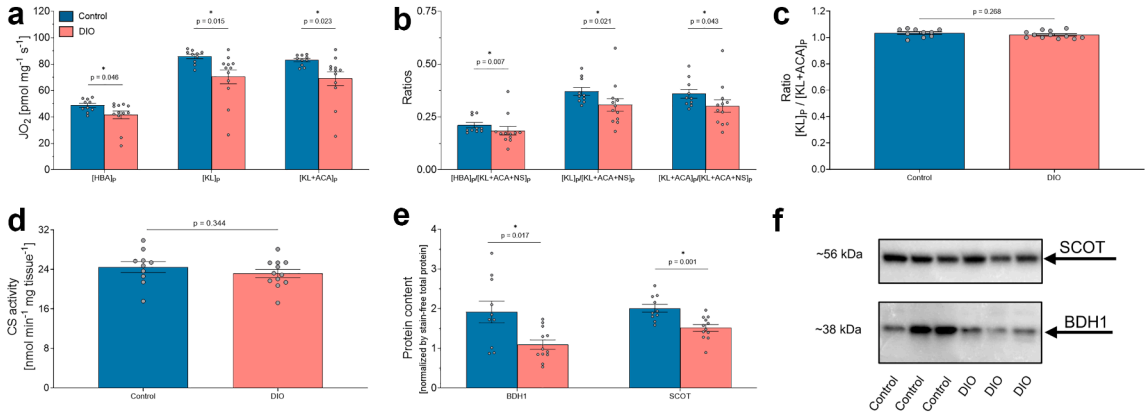

***Fig. 4:* Decreased KB-dependent OXPHOS capacity in the kidney cortex of diet-induced obesity (DIO) male mice.** (a) Mitochondrial respiration (JO_2) of permeabilised kidney cortex from DIO versus normal chow diet-fed (control) C57BL/6J male mice, obtained with the combined ketone body mitochondrial respiration protocol. (b) Relative contribution of the different respiratory states of KB-linked versus maximal coupled mitochondrial respiration determined following subsequent addition of substrates of the NADH (N) and succinate (S) pathways combined ($[KL + ACA + NS]_P$). (c) $[KL]_P/[KL + ACA]_P$ ratio. (d) Citrate Synthase (CS) activity and (e) protein expression of β-hydroxybutyrate dehydrogenase (BDH1) and succinyl-CoA: 3-ketoacid (oxoacid) coenzyme A transferase (SCOT). (f) Representative immunoblots of BDH1 and SCOT from three control and three DIO mice are shown. n = 10 versus 12. a: repeated-measurements mixed-effects (REML) model with correction for multiple testing with the false discovery rate.[74] b: multiple Mann-Whitney-tests, corrected for multiple testing with the false discovery rate.[74] c–e: Welch's t-test. Data are mean ± SEM. ACA: acetoacetate; HBA: β-hydroxybutyrate; JO_2: oxygen flux; KL: ketolysis; P: phosphorylating (coupled) mitochondrial respiration state.

Ketone body metabolism in the liver

The liver is the primary source of circulating KBs in humans for other organs through ketogenesis; this involves conversion of acetoacetyl-CoA to ACA, which is the rate limiting step of ketogenesis.[86] Correspondingly, unlike other mammalian cell types, where it is abundantly expressed, SCOT is not traceable in hepatocytes, indicating hepatocytes are not utilising ACA to generate ATP *in vivo*.[69] However, BDH1, the enzyme catalysing the equilibrium reaction between HBA and ACA (Fig. 1), is expressed in the liver to a relatively high extent.[87] Moreover, monocarboxylate transporter (MCT) 1 and other MCT proteins involved in the cellular transport of KBs are also present in hepatic tissue.[88] Thus, all prerequisites to use HBA as a substrate for mitochondrial oxidation are present in hepatocytes, even if further degradation of ACA is not possible due to a lack of SCOT.

To confirm the ability of hepatic tissue to utilise HBA as a substrate for mitochondrial oxidation *ex vivo*, we titrated HBA at saturating ADP concentrations in mouse and human liver, as we did for the other ketolytic organs. Addition of HBA as a sole substrate increased JO_2 dose-dependently, indicating that both mouse and human liver can indeed oxidise HBA *ex vivo* (Fig. 5a and b). Of note, given the liver's ketogenic nature, the JO_2 values measured in this experiment may rather reflect a non-physiological direction (HBA oxidation to ACA). Titration of HBA at saturating ADP concentrations in primary hepatocytes isolated from mouse and human livers confirms that hepatocytes can indeed catabolise HBA *ex vivo* for ATP generation (Fig. 5c and d, respectively). The JO_2 response to specific inhibitors and uncouplers added following the HBA titrations in permeabilized mouse liver, as well as in both mouse and human primary hepatocytes (Supplementary Figure S14a, b, and c, respectively) confirms that oxygen consumption in these experiments stems from mitochondrial OXPHOS via direct NADH entry through CI, as portrayed in Fig. 1. Taken together, our data demonstrate that HBA oxidation can be quantified in the liver *ex vivo* using HRR. The resulting values likely represent the enzymatic activity of BDH1 in conjunction with that of cytosolic/mitochondrial transporters linked to OXPHOS, without involvement of the TCA cycle (Fig. 1, yellow shaded area). However, whether BDH1 operates in ketolytic fashion (oxidation of HBA to ACA) *in vivo* in the liver, which is primarily a ketogenic organ,[69] remains to be determined.

As expected, titration of ACA in the presence of malate, yielded minimal (mouse) or no (human) increases in JO_2 in liver tissue (Fig. 5e and f, respectively). The lack of response to ACA in primary hepatocytes isolated from mouse and human liver (Fig. 5g and h, respectively) indicates that the minimal increases in JO_2 reported in mouse liver could be attributed to hepatic cell types other than hepatocytes, and that both murine and human hepatocytes cannot catabolise ACA for ATP generation, as expected. The minimal increase in JO_2 in mouse liver tissue may relate to recent findings demonstrating a hepatocyte-macrophage ketone shuttle, whereby liver macrophages utilise ACA as fuel substrates in a mechanism coordinating a protective fibrogenic response to hepatic injury.[16]

Lower hepatic HBA-supported mitochondrial OXPHOS capacity in MASLD

Alterations in mitochondrial function and substrate utilisation have also been observed in MASLD.[2,13] Hence, changes in the HBA-supported respiratory state in the liver could be used as a readout of variations in hepatic KB metabolism in MASLD.[2] To test this, we compared hepatic $[HBA]_P$ in obese humans with and without histologically confirmed steatosis (cut-off: $\geq$5% liver lipid content), with similar demographic and clinical characteristics (Supplementary Table S9). In participants with obesity and steatosis, hepatic $[HBA]_P$ values were lower compared to those without steatosis ($p = 0.026$; Fig. 5i), consistent with previous findings.[89] Mitochondrial respiration induced by substrates entering the ETS via the N or the NS pathway was not different between steatotic and non-steatotic hepatic tissue in this obese cohort (Fig. 5j). As a result, relative to maximal coupled OXPHOS capacity through the N pathway (which is particularly relevant in this case because the reducing equivalents generated by HBA in the liver enter the ETS only via CI in the N pathway), $[HBA]_P$ was lower in steatotic compared to non-steatotic tissue ($p = 0.002$; Fig. 5k). Similar differences were observed after normalisation by the NS pathway ($p = 0.012$; Fig. 5k). Because the steatosis but not the non-steatosis group included male participants, we conducted a sensitivity analysis restricted to females (Supplementary Figure S15), which yielded results similar as the combined-group analysis. Adjustment of JO_2 values for age and BMI using linear regression analysis produced results comparable to the unadjusted analysis (Supplementary Table S10). Considering the bidirectional nature of the equilibrium reaction catalysed by BDH1, the above findings can be interpreted as reflecting both ketolysis and ketogenesis, with the latter likely representing the more physiologically probable outcome.

In line with previous studies that have reported an increase in mitochondrial content in liver steatosis,[13] we also observed an increase CS activity in our steatosis cohort ($p = 0.034$; Fig. 5l). Following normalisation to CS activity, hepatic $[HBA]_P$ values yielded an even more pronounced reduction in the steatotic liver ($p = 0.003$; Supplementary Figure S16a), whereas OXPHOS capacity supported by the NS pathway remained not different between groups (Supplementary Figure S16b). Despite lower $[HBA]_P$ values in steatotic livers (Fig. 5i), protein expression of BDH1 did not differ between groups

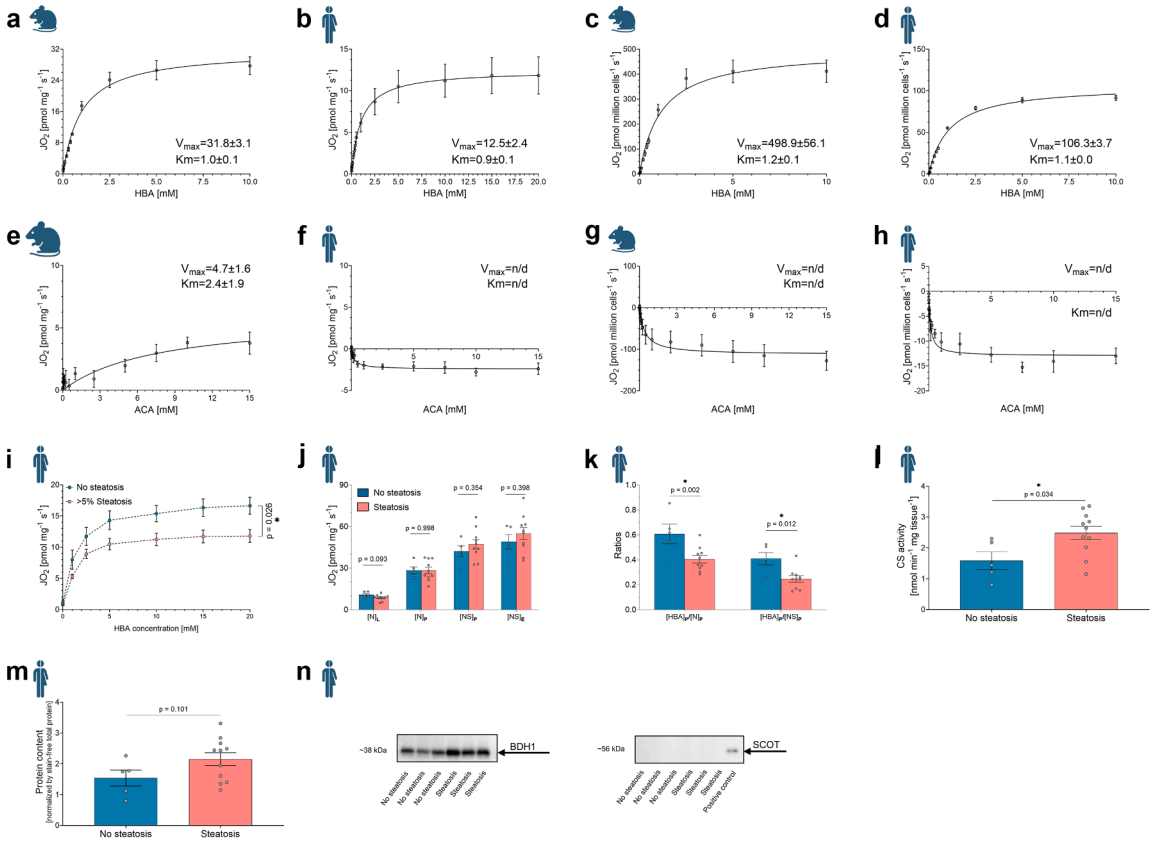

Fig. 5: **Hepatic β-hydroxybutyrate (HBA)-supported mitochondrial OXPHOS capacity is lower in individuals with steatosis.** JO_2 values from the titration of HBA in the presence of saturating levels of ADP in (a) mouse and (b) human whole-liver, and (c) mouse and (d) human primary hepatocytes with non-linear regression fits based on the mean values according to the Michaelis Menten equation. JO_2 values from the titration of acetoacetate (ACA) in the presence of saturating levels of ADP and malate in (e) mouse and (f) human whole-liver, as well as (g) mouse and (h) human primary hepatocytes with non-linear regression fits based on the mean values according to the Michaelis Menten equation. Mitochondrial respiration (JO_2) in whole-liver from participants with and without hepatic steatosis (cut-off: histological hepatic fat content >5%), obtained with (i) HBA titrations (0, 1, 2.5, 5, 10, 15, 20 mM of HBA) in the presence of saturating levels of ADP and in the absence of malate and (j) the NADH (N) and succinate (S) combined (NS) pathway mitochondrial respiration protocol. (k) Relative contribution of the $[HBA]_P$ respiratory state versus the maximal coupled N- and NS-linked mitochondrial respiration states. (l) Citrate Synthase (CS) activity and (m) protein expression of β-hydroxybutyrate dehydrogenase (BDH1). (n) Representative immunoblots of BDH1 and succinyl-CoA: 3-ketoacid (oxoacid) coenzyme A transferase (SCOT) protein expression from three replicates of each group are shown. Because SCOT is not expressed in liver tissue, a positive control was loaded on each gel to validate the suitability of the anti-SCOT antibody. a, c: n = 6. b, e, f, g: n = 7. d, h: n3. i, l, m: n = 5 versus 11, and j and k: n = 5 versus 10 for non-steatosis versus steatosis samples, respectively. Data are presented as mean ± SEM. a–h: Michaelis–Menten kinetic parameters (V_{max} and K_m values) were calculated based on the non-linear regression curve fitting and Michaelis Menten equation, and are expressed as JO_2 [pmol O_2 mg^{-1} s^{-1}]. For statistical reasons (i.e., calculation of K_m values in GraphPad Prism), the maximal KB concentration shown in panels a to h is the one inducing maximal JO_2, despite titrations continuing up to 20–40 mM HBA and 15 mM ACA, depending on species, as reported in the Methods. i: Non-linear regression curves were fitted to the data points and differences between groups were determined using repeated-measurements ANOVA. j–k: repeated-measurements mixed-effects (REML) models with correction for multiple testing with the false discovery rate.[74] l, m: Welch's t-test. D_E: electron transport chain capacity (noncoupled) mitochondrial respiration state; JO_2: oxygen flux; $_L$: leak mitochondrial respiration state; n/d: not determined; $_P$: phosphorylating (coupled) mitochondrial respiration state. Icons obtained from BioRender.com.

(Fig. 5m and n, Supplementary Figure S17), further supporting the relevance of KB respirometry protocols for investigating KB metabolism across different organs. Taken together, these findings suggest that hepatic steatosis may be associated with an increased mitochondrial content with reduced efficiency in KB metabolism.

Discussion

In the present study, we utilised KB-targeted HRR protocols to obtain a comprehensive and sensitive readout of mitochondrial KB utilisation for energy supply in specific organs in different insulin resistant states. We detected lower *ex vivo* mitochondrial KB

utilisation for ATP generation by OXPHOS in insulin resistant states in all of the organs tested.

Studies on the impact of insulin resistance on mitochondrial oxidative function and metabolic flexibility in the human heart are complicated by the shortage of safely acquirable tissue and the existing knowledge mostly relies on non-invasive methods or extrapolations from animal studies.[90] Yet, increasing evidence suggests a lower mitochondrial oxidative capacity[6,75,91] and mitochondrial metabolic inflexibility[4,90,92] in the diabetic human heart, which appears to be already detectable in prediabetic states.[70] Our data support the concept of impaired mitochondrial metabolic flexibility in the diabetic human heart by showing a reduced capacity to utilise KBs as substrates for mitochondrial OXPHOS. This reduction takes place even in the absence of significant reductions in mitochondrial OXPHOS capacity driven by substrates of the F, N and S pathways. Our results suggest that alterations of mitochondrial KB metabolism may be an early indicator of metabolic derangements in the diabetic heart.

The decrease in KB-linked OXPHOS capacity reported in the present study aligns with findings from animal studies demonstrating suppression of ketolytic enzymes in obesity or diabetes.[40,41,93] Previous studies suggest that diabetes is associated with an increase in circulating KBs and enhanced myocardial KB uptake.[33,39,90,94,95] However, although organs have been shown to extract metabolites in proportion to their circulating blood levels,[38,96] subsequent research indicates that increased KB uptake does not necessarily translate into greater KB oxidation or ATP generation in the heart.[41] This is because KB oxidation is influenced by several other factors, including the protein abundance or activity of enzymes involved in KB metabolism and the OXPHOS system, thus indicating a possible imbalance between KB supply and utilisation.[41] This underscores the value of assessing KB-linked OXPHOS capacity with respirometry, as used here, to better characterise tissue-specific pathological changes in KB metabolism in insulin-resistant states. Finally, given the evident imbalance between KB availability and utilisation, a therapeutic strategy aimed solely at increasing myocardial KB levels is unlikely to mitigate the impaired mitochondrial fuel supply in the diabetic heart.

Unlike in the heart, there is a plethora of studies examining mitochondrial OXPHOS in human skeletal muscle in insulin resistant states due to easier tissue acquisition.[7,9,78–80,97] Skeletal muscle of individuals with insulin resistance or T2D features alterations in mitochondrial quality control processes, content, and respiratory function,[2] resulting in altered mitochondrial metabolic flexibility.[2,3,5] There are discrepancies related to studies investigating changes in mitochondrial respiration in skeletal muscle of humans with T2D when this is stimulated with substrates of the NS (or FNS) pathways; while the majority of the available literature has shown that T2D is associated with a reduction in mitochondrial OXPHOS capacity,[7,9,78,79] a lack of change has also been reported,[80,97] as also indicated by our current findings. However, the present study provides evidence of a decrease in KB-linked mitochondrial OXPHOS capacity in human T2D skeletal muscle. This could be an indicator of impaired metabolic flexibility of skeletal muscle mitochondria to adapt their substrate preference. In addition, our study shows that skeletal muscle of humans with T2D exhibits also a marked decrease in the relative contribution of KB metabolism to energy production that associated with lower insulin sensitivity. Although the contribution of KB-linked mitochondrial respiration is minimal compared to classic NS pathway substrates in human skeletal muscle, as previously reported,[45] the whole-body contribution remains physiologically relevant, due to the large contribution of skeletal muscle to total body mass.[45,95]

Divergent results–both increases and decreases–have been reported for skeletal muscle KB metabolism in insulin resistant states.[34,36,42] In the present study, we observed a reduction in KB-dependent OXPHOS capacity in vastus lateralis muscle of individuals with T2D, despite no differences in BDH1 and SCOT protein expression (Fig. 3). Discrepancies among these findings are difficult to reconcile, as they likely arise from differences in species, muscle type, metabolic state, and the methodologies used to assess KB metabolism. However, the combined KB SUIT protocol employed in the present study provides a direct measure of the capacity of KBs to generate ATP, thereby offering insights into whether surrogate markers of ketolysis accurately reflect KB-dependent mitochondrial ATP production. This makes it a valuable complementary assay to the existing methods in the field, further highlighting the significance of our KB SUIT protocol. Finally, our findings question whether a therapeutic approach aimed solely at increasing skeletal muscle KB levels is able to mitigate the impaired mitochondrial fuel supply in the diabetic skeletal muscle, given its diminished ability to use KB for OXPHOS. Instead, targeting skeletal muscle mitochondrial KB metabolism directly with pharmacological or lifestyle interventions may represent a more promising approach.

KB metabolism plays a central role in the kidney, due to its almost unique ability to both produce and utilise KBs, and to the role of KBs as preferred substrates in normal physiological conditions or as readily available substrates during challenging or under fasted conditions.[11] Obesity induces a host of renal mitochondrial alterations hampering the kidney's ability to carry out its physiological functions.[11,84,98] Using designated HRR protocols, we demonstrate that diet-induced obesity resulted in a decrease in KB-linked OXPHOS

capacity in the kidney cortex of male mice, even if the capacity to generate ATP via substrates of the NS pathway remained unchanged. The decrease in HBA-linked mitochondrial respiration, as well as in BDH1 and SCOT protein content in our DIO mice is consistent with previous findings in the kidney cortex of diabetic rats demonstrating that severe hyperglycaemia is associated with significantly lower BDH1 protein content than normoglycemia, and that BDH1 protein content presents with a strong and positive correlation with plasma cystatin C,[99] a marker of renal function.[99] The present findings support the concept of impaired mitochondrial metabolic flexibility in the diabetic kidney cortex,[100] which in our study presented as early as in the obese prediabetic state. This suggests that obesity-induced derangement of renal KB metabolism may represent an early adaptation that is associated with the proven dysregulation of fatty acid metabolism, which is part of broader alterations in the metabolic landscape in the obese kidney.[84]

While the liver is primarily ketogenic and the main source of circulating KBs in humans and mice,[86] evidence exists about the ability of specific liver cells (macrophages) to utilise KBs as fuel substrates.[16] In the present study, we demonstrated that in obese humans with steatosis, HBA-supported mitochondrial respiration is significantly reduced compared with obese individuals without steatosis, both in absolute and relative terms. Even if the clinical relevance of HBA oxidation in the liver *ex vivo* remains mostly unknown, the decrease in $[HBA]_P$ in the presence of maintained NS-linked OXPHOS capacity could indicate either (i) a state of impaired ketogenesis, suggesting that $[HBA]_P$ can be utilised as a marker of hepatic functional alterations and inadequate mitochondrial adaptations in MASLD, and/or (ii) a reduced ability of liver mitochondria to generate energy from HBA (limited to the first step of ketolysis catalysed by BDH1), as previously suggested,[89] and potentially indicative of impaired mitochondrial metabolic flexibility.[101] Both, mitochondrial alterations and mitochondrial metabolic inflexibility are increasingly recognised as hallmarks of MASLD.[101–103] Future research should therefore investigate if the liver indeed oxidises HBA also *in vivo* and if this is altered

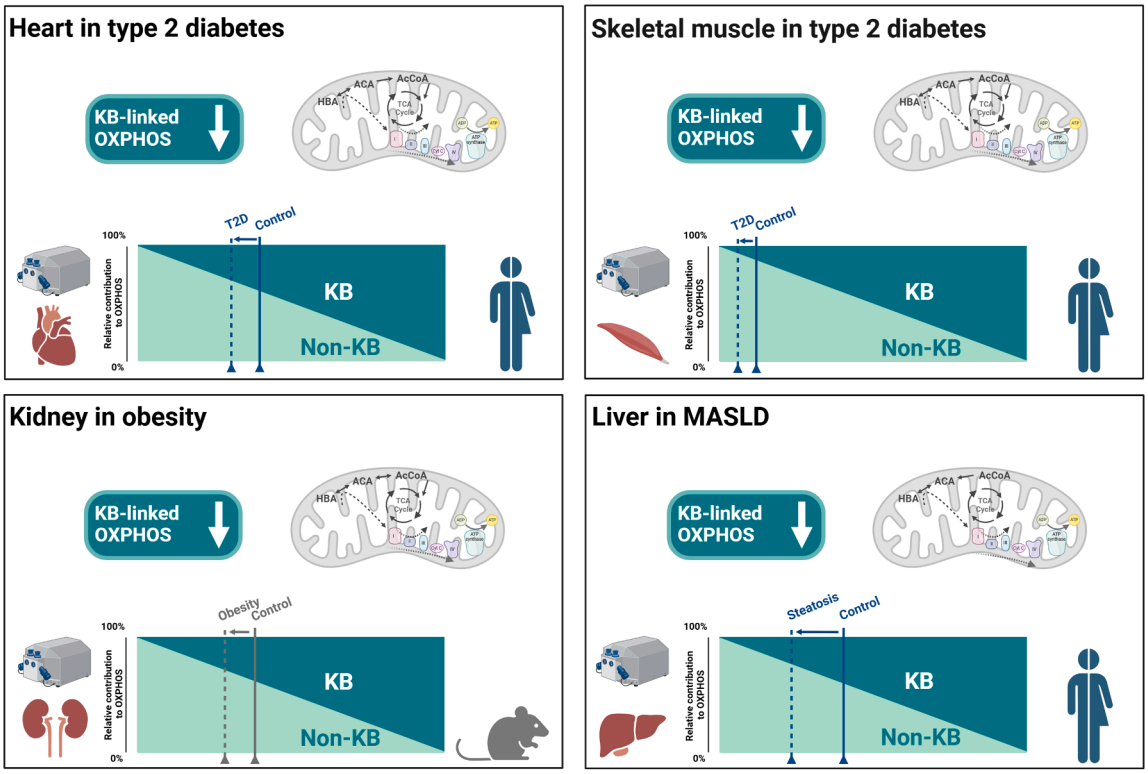

***Fig. 6:* Absolute and relative contribution of ketone body (KB)-driven mitochondrial ATP production in specific human and mouse organs in insulin resistant states.** White arrows indicate direction of change in KB-linked mitochondrial oxidative phosphorylation (OXPHOS) capacity, as described in Figs. 2–5. A downward arrow indicates a decrease. The solid and dotted lines in the rectangles in each quadrant represent the relative contribution of KB-driven OXPHOS capacity to maximal OXPHOS capacity, as determined in Figs. 2–5 for control and diseased cohorts, respectively. Blue lines indicate human cohorts, grey lines indicate mouse cohorts. ACA: acetoacetate; AcCoA: acetyl coenzyme A; HBA: β-hydroxybutyrate; T2D: type 2 diabetes; TCA: tricarboxylic acid. Figure generated using BioRender.com.

during progression of MASLD. Such studies will have the potential to identify novel pathways to target the not yet fully met need to reverse liver fibrosis.

By integrating findings from our combined KB SUIT protocol and the classic NS (or FNS) pathway protocol, our approach enabled the characterisation of the relative contribution of KB metabolism to maximal coupled OXPHOS capacity driven by OXPHOS substrates of the F, N and S pathways in several pathophysiological insulin resistant states in different species and organs (Fig. 6). Correspondingly, the present study specifically investigates the contribution of ketolysis to mitochondrial OXPHOS capacity in the human type 2 diabetic cardiac and skeletal muscle, the mouse diet-induced obese kidney, and the human steatotic liver. As shown in Fig. 6, metabolic conditions characterised by insulin resistance were associated with a reduction in the contribution of KBs to the overall capacity to generate ATP via OXPHOS in all tissues analysed, which may reflect the metabolic landscape associated with systemic insulin resistance. Our findings highlight the involvement of KB metabolism as a potential cause or consequence underlying insulin resistance and suggests that modulation of KB metabolism may represent a promising therapeutic avenue for this condition.

One of the main advantages of utilising HRR to determine KB-linked mitochondrial respiration is that the readouts reflect the integrated functionality of the various processes involved in mitochondrial KB metabolism, including KB uptake into mitochondria, mitochondrial ketolysis, transport of reducing equivalents to the OXPHOS system, and the final generation of ATP via OXPHOS. This technique offers a sensitive readout of KB-related mitochondrial functional impairments and a more complete picture of KB metabolism than other currently used spot readouts, such as determination of a single enzyme content or activity, the amount of circulating KBs, or individual KBs uptake by specific organs, as HRR is performed in whole-tissue in a fully functional mitochondrial system.[29,30,35,45]

Limitations

Ethical and practical constraints on obtaining the different human tissues limited access to broader populations and other organs. Consequently, our clinically relevant cohorts including heart-transplant recipients and persons with obesity undergoing bariatric surgery limit the generalisability of the findings, calling for their validation in larger different cohorts, across additional organs and disease states. Particularly, we were not able to source human kidney, which limited our examination of renal KB metabolism to a rodent model of obesity. It is also important to underline that despite the abovementioned advantages of using HRR to determine KB metabolism, the results presented herein need to be interpreted as the maximal stimulable OXPHOS capacity in a laboratory apparatus where ADP and oxygen are present at saturating concentrations, and in the absence of other substrates stimulating OXPHOS capacity via different pathways. Although this is the case for most laboratory analyses, as well as for HRR protocols with classic F, N, and S pathway substrates, it is important to underline that these results may not completely mirror an *in vivo* situation. Finally, although confounding was controlled for in the human cohorts with respect to age, BMI, and sex, residual confounding factors cannot be excluded.

Conclusion

In conclusion, we demonstrated that distinct pathophysiological states of insulin resistance, such as T2D, obesity, and MASLD are associated with a reduction in KB-driven mitochondrial OXPHOS capacity across different organs. Our results begin to fill the evident gap of previous literature that was limited to the assessment of single aspects of KB metabolism or simple KB uptake. In addition, our findings may suggest that in insulin resistant states—such as diabetic cardiac or skeletal muscle, the steatotic liver, or the obese kidney—targeting tissue-specific KB OXPHOS capacity and mitochondrial metabolic flexibility may be a more promising and valuable therapeutic approach than increasing circulating KB levels. The findings provided herein pave the way for new research investigating the potential of therapeutic strategies targeting the modulation of KB utilisation in these pathologies.

Contributors

Conceptualisation and Methodology: EZ, SP, AP, JS, MR, and CG. Investigation: EZ, SP, JWS, RR, and CG. Resources: EZ, SP, JWS, DS, MS, SK, VB, BD, RR, AC, HA-H, HA, UB, AL, AP, MK, RaW, RoW, PS, JS, MR, and CG. Data curation, formal analysis and visualisation: EZ, JWS, SP, LM, and CG. Writing–Original Draft: EZ, SP, and CG. Funding acquisition: EZ, JS, RaW and MR. Writing–Review & Editing: all authors reviewed the manuscript critically and approved the final version. EZ, SP, MR, and CG accessed and verified the underlying data of this manuscript.

Data sharing statement

The datasets used and/or analysed during the current study are available from the corresponding author upon request.

Declaration of interests

AP receives research funding from Abiomed, consulting fees from Bayer, Bristol Myers Squibb, Boehringer Ingelheim, Pfizer, and Sanofi, honoraria for lectures, presentations, or similar activities from Abbott, Abiomed, Amarin, AstraZeneca, Bayer, Bristol Myers Squibb, Corvia Medical, Daiichi Sancho, Edwards, Medtronic, Occlutech, Pfizer, Philips and meeting support from Bayer. JD has consultancy relationships with Active Biotech, Anamar, ARXX, AstraZeneca, Bayer Pharma, Boehringer Ingelheim, Callidatas, Calluna, Galapagos, GSK, Janssen, Kyverna, Ono Pharmaceutical, Merck, Novartis, Quell Therapeutics, Tyra and UCB and receives research funding from Anamar, AstraZeneca, ARXX, BMS, Boehringer Ingelheim, Cantargia, Celgene, CSL Behring, Exo Therapeutics, Galapagos, GSK, Incyte, Inventiva, Kiniksa, Kyverna, Lassen Therapeutics, Mestag, Sanofi-Aventis, SpicaTx, RedX, UCB and ZenasBio, as well as writing support from Boehringer-Ingelheim and Endeavour Biosciencesa and meeting support from AbbVie and SoBi. JHWD is CEO of 4D Science and scientific lead of FibroCure. RaW is employed by Abiomed. RoW reports lecture fees

from Novo Nordisk, Sanofi-Aventis, Boehringer Ingelheim and Eli Lilly, and served on the advisory board for Akcea Therapeutics, Daiichi Sankyo, Sanofi-Aventis, Eli Lilly, and NovoNordisk. MR is currently on scientific advisory boards of Astra Zeneca, Boehringer Ingelheim, Echosens, Eli Lilly, Madrigal, Merck-MSD, Novo Nordisk, and Target RWE, and has received support for investigator-initiated studies from Boehringer Ingelheim, Novo Nordisk and Nutricia/Danone. PS is on scientific advisory boards of Rivus and AstraZeneca, and has received support for investigator-initiated studies from AstraZeneca, Pfizer and MedImmune. CG is an Adjunct Research Fellow at Monash University (Melbourne, Australia). SP has filed patent applications for the use of protected carboxylic acid-based metabolites for treatment of mitochondrial disorders (WO/2017/060400, WO/2017/060,418, WO/2017/060422). The other authors declare no competing interests.

Acknowledgements

We would like to thank Julius Borger, Fariba Zivehe, Olga Dürrschmidt, Alexandra Stein, Michelle Reina do Fundo, and Jan-Marc Leonhard for their help in mouse and tissue handling, and for performing respirometry. We acknowledge Dr Klaus Straßburger for his statistical expertise, and the support of the Susanne-Bunnenberg-Stiftung at the Düsseldorf Heart Center. We acknowledge the support of the GDS. The German Diabetes Study (GDS) Group consists of M. Roden (speaker), H. Al-Hasani, B. Belgardt, G. Bönhof, G. Geerling, C. Herder, A. Icks, K. Jandeleit-Dahm, J. Kotzka, O. Kuß, E. Lammert, W. Rathmann, S. Schlesinger, V. Schrauwen-Hinderling, S. Trenkamp, R. Wagner and their co-workers who are responsible for the design and conduct of the GDS. This work is supported by grants from the German Research Foundation (Deutsche Forschungsgemeinschaft; DFG) (CRC1116, grant number 236177352) and by the German Diabetes Center (DDZ), which is funded by the German Federal Ministry of Health (BMG) and the Ministry of Culture and Science of the State of North Rhine-Westphalia (MKW NRW) and receives grants by the German Center for Diabetes Research (DZD e.V.), which is funded by the German Federal Ministry of Education and Research (BMBF) and by the MKW NRW. The work of EZ is supported by grants from the DFG (numbers 527448911, 493659010), the German Heart Foundation (F/22/18), the German Diabetes Society (DDG) (Menarini research grant 2020), and the Christiane-and-Claudia Hempel Foundation. The work of MR is further supported by grants from the European Community (HORIZON-HLTH-2022-STAYHLTH-02-01: Panel A) to the INTERCEPT-T2D consortium and the Schmutzler-Stiftung to the DDZ.

Appendix A. Supplementary data

Supplementary data related to this article can be found at https://doi.org/10.1016/j.ebiom.2025.106007.

References

1 Tsilingiris D, Tzeravini E, Koliaki C, Dalamaga M, Kokkinos A. The role of mitochondrial adaptation and metabolic flexibility in the pathophysiology of obesity and insulin resistance: an updated overview. *Curr Obes Rep*. 2021;10(3):191–213.
2 Georgiev A, Granata C, Roden M. The role of mitochondria in the pathophysiology and treatment of common metabolic diseases in humans. *Am J Physiol Cell Physiol*. 2022;322(6):C1248–C1259.
3 Szendroedi J, Phielix E, Roden M. The role of mitochondria in insulin resistance and type 2 diabetes mellitus. *Nat Rev Endocrinol*. 2011;8(2):92–103.
4 Makrecka-Kuka M, Liepinsh E, Murray AJ, et al. Altered mitochondrial metabolism in the insulin-resistant heart. *Acta Physiol*. 2020;228(3):e13430.
5 Roden M, Shulman GI. The integrative biology of type 2 diabetes. *Nature*. 2019;576(7785):51–60.
6 Zweck E, Scheiber D, Jelenik T, et al. Exposure to type 2 diabetes provokes mitochondrial impairment in apparently healthy human hearts. *Diabetes Care*. 2021;44(5):e82–e84.
7 Phielix E, Schrauwen-Hinderling VB, Mensink M, et al. Lower intrinsic ADP-stimulated mitochondrial respiration underlies in vivo mitochondrial dysfunction in muscle of male type 2 diabetic patients. *Diabetes*. 2008;57(11):2943–2949.
8 Bakkman L, Fernström M, Loogna P, Rooyackers O, Brandt L, Lagerros YT. Reduced respiratory capacity in muscle mitochondria of obese subjects. *Obes Facts*. 2010;3(6):371–375.
9 Mogensen M, Sahlin K, Fernström M, et al. Mitochondrial respiration is decreased in skeletal muscle of patients with type 2 diabetes. *Diabetes*. 2007;56(6):1592–1599.
10 Boushel R, Gnaiger E, Schjerling P, Skovbro M, Kraunsøe R, Dela F. Patients with type 2 diabetes have normal mitochondrial function in skeletal muscle. *Diabetologia*. 2007;50(4):790–796.
11 Forbes JM, Thorburn DR. Mitochondrial dysfunction in diabetic kidney disease. *Nat Rev Nephrol*. 2018;14(5):291–312.
12 Munusamy S, do Carmo JM, Hosler JP, Hall JE. Obesity-induced changes in kidney mitochondria and endoplasmic reticulum in the presence or absence of leptin. *Am J Physiol Renal Physiol*. 2015;309(8):F731–F743.
13 Koliaki C, Szendroedi J, Kaul K, et al. Adaptation of hepatic mitochondrial function in humans with non-alcoholic fatty liver is lost in steatohepatitis. *Cell Metab*. 2015;21(5):739–746.
14 Sanyal AJ, Campbell-Sargent C, Mirshahi F, et al. Nonalcoholic steatohepatitis: association of insulin resistance and mitochondrial abnormalities. *Gastroenterology*. 2001;120(5):1183–1192.
15 Puchalska P, Crawford PA. Metabolic and signaling roles of ketone bodies in health and disease. *Annu Rev Nutr*. 2021;41:49–77.
16 Puchalska P, Martin SE, Huang X, et al. Hepatocyte-Macrophage acetoacetate shuttle protects against tissue fibrosis. *Cell Metab*. 2019;29(2):383–398.e7.
17 Cho IY, Chang Y, Sung E, et al. Fasting ketonuria is inversely associated with coronary artery calcification in non-diabetic individuals. *Atherosclerosis*. 2022;348:1–7.
18 Homilius C, Seefeldt JM, Axelsen JS, et al. Ketone body 3-hydroxybutyrate elevates cardiac output through peripheral vasorelaxation and enhanced cardiac contractility. *Basic Res Cardiol*. 2023;118(1):37.
19 Nielsen R, Møller N, Gormsen LC, et al. Cardiovascular effects of treatment with the ketone body 3-Hydroxybutyrate in chronic heart failure patients. *Circulation*. 2019;139(18):2129–2141.
20 Horton JL, Davidson MT, Kurishima C, et al. The failing heart utilizes 3-hydroxybutyrate as a metabolic stress defense. *JCI Insight*. 2019;4(4):e124079.
21 Berg-Hansen K, Christensen KH, Gopalasingam N, et al. Beneficial effects of ketone ester in patients with cardiogenic shock: a randomized, controlled, double-blind trial. *JACC Heart Fail*. 2023;11(10):1337–1347.
22 Hørsdal OK, Larsen AM, Wethelund KL, et al. The ketone body 3-hydroxybutyrate increases cardiac output and cardiac contractility in a porcine model of cardiogenic shock: a randomized, blinded, crossover trial. *Basic Res Cardiol*. 2025;120(3):579–596.
23 Henderson ST, Vogel JL, Barr LJ, Garvin F, Jones JJ, Costantini LC. Study of the ketogenic agent AC-1202 in mild to moderate Alzheimer's disease: a randomized, double-blind, placebo-controlled, multicenter trial. *Nutr Metab*. 2009;6:31.
24 Koyuncu H, Fidan V, Toktas H, Binay O, Celik H. Effect of ketogenic diet versus regular diet on voice quality of patients with Parkinson's disease. *Acta Neurol Belg*. 2021;121(6):1729–1732.
25 Tomita I, Kume S, Sugahara S, et al. SGLT2 inhibition mediates protection from diabetic kidney disease by promoting ketone body-induced mTORC1 inhibition. *Cell Metab*. 2020;32(3):404–419.e6.
26 Jung J, Park WY, Kim YJ, et al. 3-Hydroxybutyrate ameliorates the progression of diabetic nephropathy. *Antioxidants (Basel)*. 2022;11(2):381.
27 Chen J, Li Z, Zhang Y, et al. Mechanism of reduced muscle atrophy via ketone body (D)-3-hydroxybutyrate. *Cell Biosci*. 2022;12(1):94.
28 Li J, Zhang H, Dai Z. Cancer treatment with the Ketogenic diet: a systematic review and meta-analysis of animal studies. *Front Nutr*. 2021;8:594408.
29 Cox PJ, Kirk T, Ashmore T, et al. Nutritional ketosis alters fuel preference and thereby endurance performance in athletes. *Cell Metab*. 2016;24(2):256–268.
30 Huang D, Li T, Wang L, et al. Hepatocellular carcinoma redirects to ketolysis for progression under nutrition deprivation stress. *Cell Res*. 2016;26(10):1112–1130.
31 Abdurrachim D, Teo XQ, Woo CC, et al. Empagliflozin reduces myocardial ketone utilization while preserving glucose utilization in diabetic hypertensive heart disease: a hyperpolarized (13) C magnetic resonance spectroscopy study. *Diabetes Obes Metab*. 2019;21(2):357–365.

32 Soeters MR, Sauerwein HP, Faas L, et al. Effects of insulin on ketogenesis following fasting in lean and obese men. *Obesity (Silver Spring)*. 2009;17(7):1326–1331.
33 Singh BM, Krentz AJ, Nattrass M. Insulin resistance in the regulation of lipolysis and ketone body metabolism in non-insulin dependent diabetes is apparent at very low insulin concentrations. *Diabetes Res Clin Pract*. 1993;20(1):55–62.
34 Vice E, Privette JD, Hickner RC, Barakat HA. Ketone body metabolism in lean and obese women. *Metabolism*. 2005;54(11):1542–1545.
35 Santos-Gallego CG, Requena-Ibanez JA, San Antonio R, et al. Empagliflozin ameliorates adverse left ventricular remodeling in nondiabetic heart failure by enhancing myocardial energetics. *J Am Coll Cardiol*. 2019;73(15):1931–1944.
36 Al Batran R, Gopal K, Capozzi ME, et al. Pimozide alleviates hyperglycemia in diet-induced obesity by inhibiting skeletal muscle ketone oxidation. *Cell Metab*. 2020;31(5):909–919.e8.
37 Khouri H, Roberge M, Ussher JR, Aguer C. Acetoacetate and d- and l-β-hydroxybutyrate have distinct effects on basal and insulin-stimulated glucose uptake in L6 skeletal muscle cells. *Am J Physiol Cell Physiol*. 2024;326(6):C1710–C1720.
38 Mikkelsen KH, Seifert T, Secher NH, Grøndal T, van Hall G. Systemic, cerebral and skeletal muscle ketone body and energy metabolism during acute Hyper-D-β-Hydroxybutyratemia in post-absorptive healthy males. *J Clin Endocrinol Metab*. 2015;100(2):636–643.
39 Hall SE, Wastney ME, Bolton TM, Braaten JT, Berman M. Ketone body kinetics in humans: the effects of insulin-dependent diabetes, obesity, and starvation. *J Lipid Res*. 1984;25(11):1184–1194.
40 Cai W, Chong K, Huang Y, Huang C, Yin L. Empagliflozin improves mitochondrial dysfunction in diabetic cardiomyopathy by modulating ketone body metabolism and oxidative stress. *Redox Biol*. 2024;69:103010.
41 Brahma MK, Ha CM, Pepin ME, et al. Increased glucose availability attenuates myocardial ketone body utilization. *J Am Heart Assoc*. 2020;9(15):e013039.
42 Soni S, Tabatabaei Dakhili SA, Ussher JR, Dyck JRB. The therapeutic potential of ketones in cardiometabolic disease: impact on heart and skeletal muscle. *Am J Physiol Cell Physiol*. 2024;326(2):C551–C566.
43 Pesta D, Gnaiger E. High-resolution respirometry: OXPHOS protocols for human cells and permeabilized fibers from small biopsies of human muscle. *Methods Mol Biol*. 2012;810:25–58.
44 Granata C, Jamnick NA, Bishop DJ. Training-Induced changes in mitochondrial content and respiratory function in human skeletal muscle. *Sports Med*. 2018;48(8):1809–1828.
45 Petrick HL, Brunetta HS, Pignanelli C, et al. In vitro ketone-supported mitochondrial respiration is minimal when other substrates are readily available in cardiac and skeletal muscle. *J Physiol*. 2020;598(21):4869–4885.
46 Zweck E, Karschnia M, Scheiber D, et al. Receptor autoantibodies: associations with cardiac markers, histology, and function in human non-ischaemic heart failure. *ESC Heart Fail*. 2023;10(2):1258–1269.
47 Scheiber D, Jelenik T, Zweck E, et al. High-resolution respirometry in human endomyocardial biopsies shows reduced ventricular oxidative capacity related to heart failure. *Exp Mol Med*. 2019;51(2):1–10.
48 Szendroedi J, Saxena A, Weber KS, et al. Cohort profile: the German Diabetes Study (GDS). *Cardiovasc Diabetol*. 2016;15:59.
49 ElSayed NA, McCoy RG, Aleppo G, et al. Diagnosis and classification of diabetes: standards of care in Diabetes—2025. *Diabetes Care*. 2024;48(Supplement_1):S27–S49.
50 Tura A, Chemello G, Szendroedi J, et al. Prediction of clamp-derived insulin sensitivity from the oral glucose insulin sensitivity index. *Diabetologia*. 2018;61(5):1135–1141.
51 Martins T, Ferreira T, Nascimento-Gonçalves E, et al. Obesity rodent models applied to research with food products and natural compounds. *Obesities*. 2022;2(2):171–204.
52 Avtanski D, Pavlov VA, Tracey KJ, Poretsky L. Characterization of inflammation and insulin resistance in high-fat diet-induced male C57BL/6J mouse model of obesity. *Animal Model Exp Med*. 2019;2(4):252–258.
53 Juszczak F, Pierre L, Decarnoncle M, et al. Sex differences in obesity-induced renal lipid accumulation revealed by lipidomics: a role of adiponectin/AMPK axis. *Biol Sex Differ*. 2023;14(1):63.
54 Charan J, Kantharia ND. How to calculate sample size in animal studies? *J Pharmacol Pharmacother*. 2013;4(4):303–306.
55 Hu J, Srivastava K, Wieland M, et al. Endothelial cell-derived angiopoietin-2 controls liver regeneration as a spatiotemporal rheostat. *Science*. 2014;343(6169):416–419.
56 Dropmann A, Dewidar B, Gould K, et al. CD271 sorting for improved liver cell isolation: semiautomated and simultaneous preparation of parenchymal and non-parenchymal cells from mouse and human livers. *bioRxiv*. 2025. https://doi.org/10.1101/2025.01.21.633876.
57 LeCluyse EL, Alexandre E, Hamilton GA, et al. Isolation and culture of primary human hepatocytes. *Methods Mol Biol*. 2005;290:207–229.
58 Scheiber D, Zweck E, Jelenik T, et al. Reduced myocardial mitochondrial ROS production in mechanically unloaded hearts. *J Cardiovasc Transl Res*. 2019;12(2):107–115.
59 Dewidar B, Mastrototaro L, Englisch C, et al. Alterations of hepatic energy metabolism in murine models of obesity, diabetes and fatty liver diseases. *eBioMedicine*. 2023;94:104714.
60 Lund MT, Kristensen M, Hansen M, et al. Hepatic mitochondrial oxidative phosphorylation is normal in obese patients with and without type 2 diabetes. *J Physiol*. 2016;594(15):4351–4358.
61 Granata C, Caruana NJ, Botella J, et al. High-intensity training induces non-stoichiometric changes in the mitochondrial proteome of human skeletal muscle without reorganisation of respiratory chain content. *Nat Commun*. 2021;12(1):7056.
62 Parajuli N, Shrum S, Tobacyk J, Harb A, Arthur JM, MacMillan-Crow LA. Renal cold storage followed by transplantation impairs expression of key mitochondrial fission and fusion proteins. *PLoS One*. 2017;12(10):e0185542.
63 Piel S, Chamkha I, Dehlin AK, et al. Cell-permeable succinate prodrugs rescue mitochondrial respiration in cellular models of acute acetaminophen overdose. *PLoS One*. 2020;15(4):e0231173.
64 Granata C, Oliveira RS, Little JP, Renner K, Bishop DJ. Mitochondrial adaptations to high-volume exercise training are rapidly reversed after a reduction in training volume in human skeletal muscle. *FASEB J*. 2016;30(10):3413–3423.
65 Granata C, Oliveira RS, Little JP, Renner K, Bishop DJ. Training intensity modulates changes in PGC-1alpha and p53 protein content and mitochondrial respiration, but not markers of mitochondrial content in human skeletal muscle. *FASEB J*. 2016;30(2):959–970.
66 Kuang J, Saner NJ, Botella J, et al. Assessing mitochondrial respiration in permeabilized fibres and biomarkers for mitochondrial content in human skeletal muscle. *Acta Physiol (Oxf)*. 2022;234(2):e13772.
67 Fritzsche I, Bührdel P, Melcher R, Böhme HJ. Stability of ketone bodies in serum in dependence on storage time and storage temperature. *Clin Lab*. 2001;47(7–8):399–403.
68 Gnaiger E. *Mitochondrial pathways and respiratory control: an introduction to OXPHOS analysis; Mitochondr Physiol Network 17.18: Oroboros Instruments*. 2012.
69 Fukao T, Song XQ, Mitchell GA, et al. Enzymes of ketone body utilization in human tissues: protein and messenger RNA levels of succinyl-coenzyme A (CoA):3-ketoacid CoA transferase and mitochondrial and cytosolic acetoacetyl-CoA thiolases. *Pediatr Res*. 1997;42(4):498–502.
70 Zweck E, Scheiber D, Schultheiss HP, et al. Impaired myocardial mitochondrial respiration in humans with prediabetes: a footprint of prediabetic cardiomyopathy. *Circulation*. 2022;146(15):1189–1191.
71 Morgunov I, Srere PA. Interaction between citrate synthase and malate dehydrogenase. Substrate channeling of oxaloacetate. *J Biol Chem*. 1998;273(45):29540–29544.
72 Apostolopoulou M, Mastrototaro L, Hartwig S, et al. Metabolic responsiveness to training depends on insulin sensitivity and protein content of exosomes in insulin-resistant males. *Sci Adv*. 2021;7(41):eabi9551.
73 Pafili K, Kahl S, Mastrototaro L, et al. Mitochondrial respiration is decreased in visceral but not subcutaneous adipose tissue in obese individuals with fatty liver disease. *J Hepatol*. 2022;77(6):1504–1514.
74 Benjamini Y, Krieger AM, Yekutieli D. Adaptive linear step-up procedures that control the false discovery rate. *Biometrika*. 2006;93(3):491–507.
75 Montaigne D, Marechal X, Coisne A, et al. Myocardial contractile dysfunction is associated with impaired mitochondrial function and dynamics in type 2 diabetic but not in obese patients. *Circulation*. 2014;130(7):554–564.

76 Anderson EJ, Kypson AP, Rodriguez E, Anderson CA, Lehr EJ, Neufer PD. Substrate-specific derangements in mitochondrial metabolism and redox balance in the atrium of the type 2 diabetic human heart. *J Am Coll Cardiol*. 2009;54(20):1891–1898.
77 American Diabetes Association. 2. Classification and diagnosis of diabetes: standards of medical care in Diabetes-2021. *Diabetes Care*. 2021;44(Suppl 1):S15–S33.
78 Rabøl R, Larsen S, Højberg PM, et al. Regional anatomic differences in skeletal muscle mitochondrial respiration in type 2 diabetes and obesity. *J Clin Endocrinol Metab*. 2010;95(2):857–863.
79 Szendroedi J, Schmid AI, Chmelik M, et al. Muscle mitochondrial ATP synthesis and glucose transport/phosphorylation in type 2 diabetes. *PLoS Med*. 2007;4(5):e154.
80 Lund MT, Larsen S, Hansen M, et al. Mitochondrial respiratory capacity remains stable despite a comprehensive and sustained increase in insulin sensitivity in obese patients undergoing gastric bypass surgery. *Acta Physiol (Oxf)*. 2018;223(1):e13032.
81 Larsen S, Nielsen J, Hansen CN, et al. Biomarkers of mitochondrial content in skeletal muscle of healthy young human subjects. *J Physiol*. 2012;590(14):3349–3360.
82 Liu H, Yan L-J. The role of ketone bodies in various animal models of kidney disease. *Endocrines*. 2023;4(1):236–249.
83 Coughlan MT, Nguyen TV, Penfold SA, et al. Mapping time-course mitochondrial adaptations in the kidney in experimental diabetes. *Clin Sci*. 2016;130(9):711–720.
84 D'Agati VD, Chagnac A, de Vries AP, et al. Obesity-related glomerulopathy: clinical and pathologic characteristics and pathogenesis. *Nat Rev Nephrol*. 2016;12(8):453–471.
85 Kleinert M, Clemmensen C, Hofmann SM, et al. Animal models of obesity and diabetes mellitus. *Nat Rev Endocrinol*. 2018;14(3):140–162.
86 Laffel L. Ketone bodies: a review of physiology, pathophysiology and application of monitoring to diabetes. *Diabetes Metab Res Rev*. 1999;15(6):412–426.
87 Männistö VT, Simonen M, Hyysalo J, et al. Ketone body production is differentially altered in steatosis and non-alcoholic steatohepatitis in obese humans. *Liver Int*. 2015;35(7):1853–1861.
88 Puchalska P, Crawford PA. Multi-dimensional roles of ketone bodies in fuel metabolism, signaling, and therapeutics. *Cell Metab*. 2017;25(2):262–284.
89 Fletcher JA, Deja S, Satapati S, Fu X, Burgess SC, Browning JD. Impaired ketogenesis and increased acetyl-CoA oxidation promote hyperglycemia in human fatty liver. *JCI Insight*. 2019;5(11):e127737.
90 Bornstein MR, Tian R, Arany Z. Human cardiac metabolism. *Cell Metab*. 2024;36(7):1456–1481.
91 Duicu OM, Lighezan R, Sturza A, et al. Assessment of mitochondrial dysfunction and monoamine oxidase contribution to oxidative stress in human diabetic hearts. *Oxid Med Cell Longev*. 2016;2016:8470394.
92 Gambardella J, Lombardi A, Santulli G. Metabolic flexibility of Mitochondria plays a key role in balancing glucose and fatty acid metabolism in the diabetic heart. *Diabetes*. 2020;69(10):2054–2057.
93 Verma S, Rawat S, Ho KL, et al. Empagliflozin increases cardiac energy production in diabetes: novel translational insights into the heart failure benefits of SGLT2 inhibitors. *JACC Basic Transl Sci*. 2018;3(5):575–587.
94 Mizuno Y, Harada E, Nakagawa H, et al. The diabetic heart utilizes ketone bodies as an energy source. *Metabolism*. 2017;77:65–72.
95 Robinson AM, Williamson DH. Physiological roles of ketone bodies as substrates and signals in mammalian tissues. *Physiol Rev*. 1980;60(1):143–187.
96 Funada J, Betts TR, Hodson L, et al. Substrate utilization by the failing human heart by direct quantification using arterio-venous blood sampling. *PLoS One*. 2009;4(10):e7533.
97 Monaco CMF, Tarnopolsky MA, Dial AG, et al. Normal to enhanced intrinsic mitochondrial respiration in skeletal muscle of middle- to older-aged women and men with uncomplicated type 1 diabetes. *Diabetologia*. 2021;64(11):2517–2533.
98 Hamada S, Takata T, Yamada K, et al. Steatosis is involved in the progression of kidney disease in a high-fat-diet-induced non-alcoholic steatohepatitis mouse model. *PLoS One*. 2022;17(3):e0265461.
99 Granata C, Thallas-Bonke V, Caruana NJ, et al. Deep multi-omic profiling reveals extensive mitochondrial remodeling driven by glycemia in early diabetic kidney disease. *bioRxiv*. 2023. https://doi.org/10.1101/2023.10.26.564228.
100 Czajka A, Ajaz S, Gnudi L, et al. Altered mitochondrial function, mitochondrial DNA and reduced metabolic flexibility in patients with diabetic nephropathy. *eBioMedicine*. 2015;2(6):499–512.
101 Hyötyläinen T, Jerby L, Petäjä EM, et al. Genome-scale study reveals reduced metabolic adaptability in patients with non-alcoholic fatty liver disease. *Nat Commun*. 2016;7:8994.
102 Targher G, Corey KE, Byrne CD, Roden M. The complex link between NAFLD and type 2 diabetes mellitus - mechanisms and treatments. *Nat Rev Gastroenterol Hepatol*. 2021;18(9):599–612.
103 Fromenty B, Roden M. Mitochondrial alterations in fatty liver diseases. *J Hepatol*. 2023;78(2):415–429.